YRKESHÖGSKOLAN
NOVIA

Development of a Low-Cost Solar Data Logger Using a PV Panel

Gabriel Bálint

Degree thesis for Bachelor of Engineering

Degree Programme in Energy Technology

Vaasa, Finland, 2022

DEGREE THESIS

Author: Gabriel Bálint
Degree Programme and place of study: Electrical engineering and automation, Lleida
Specialisation: Energy Technology
Supervisors: Hans Lindén and Philip Hollins

Title: Development of a low-cost solar data logger using a PV panel

---

Date: 26.08.2022 Number of pages: 56 Appendices: 6

Abstract

With the increased popularity and lower cost of PV panels, Novia University of Applied Sciences is planning to install a PV system on the roof of the university building. This thesis aimed to create a low-cost solar data logger for the project's feasibility study.

The device created uses an ESP32 as a controller and logs the data through MQTT protocol. The sensor is based on a 5 W PV panel and uses an INA219 combined with a MOSFET-based electronic load to obtain the partial I-V characteristics in under five seconds with a resolution of 64 I-V data points. This data allows quantifying the ideality of the environmental conditions for PV power generation. The logger is battery-powered and can use PV power to recharge the battery.

The manufacturing of a prototype was partially done. The short-term operation in laboratory conditions was validated. Long-term outdoors testing of a complete model and validating the measured magnitude are pending. The manufacturing cost of a prototype is estimated to be about 75 €.

The concept of this device is an interesting alternative to traditional pyranometers, which measure solar irradiance and can prove to be useful to assess potential areas of PV power harvesting or monitor already existing systems.

Language: English
Key Words: Data logger, I-V characterisation, ESP32, MQTT, INA219

Table of Contents

List of Figures

List of Tables

Glossary

3D	Three Dimensional
ADC	Analog to Digital Converter
BJT	Bipolar Junction Transistor
DAC	Digital to Analog Converter
GHI	Global Horizontal Irradiance
GPIO	General Purpose Input/Output
HTTP	Hypertext Transfer Protocol
IDE	Integrated Development Environment
IoT	Internet of Things
JSON	JavaScript Object Notation
LDR	Light-Dependant Resistor
MOSFET	Metal Oxide Semiconductor Field Effect Transistor
MPP	Maximum Power Point
MQTT	Message Queuing Telemetry Transport
NTP	Network Time Protocol
NVS	Non-Volatile Storage
PCB	Printed Circuit Board
PD	Photodiode
PETg	Polyethylene Terephthalate Glycol
PT	Phototransistor
PV	Photovoltaic
RTC	Real-Time Clock
SBW	Spectral Bandwidth
SMT	Surface Mount Technology
SNTP	Simple Network Time Protocol
SoC	System on Chip
THT	Through-Hole Technology
UV	Ultraviolet

1 Introduction

This section discusses general information about the thesis, including the general background and motivation, the aim and objectives, and the document's structure.

1.1 Background

The use of solar photovoltaic (PV) panels has increased in popularity due to a drop in purchase price and an increase in relative operating efficiency (IRENA, 2021). However, installing PV panels needs some planning to assure their optimum performance in each scenario or to decide if it is even worth it.

Feasibility studies are conducted in most cases, especially for large-scale installations, to guarantee that the project is economically, technically, and legally viable. Part of these studies requires data on the solar radiation (irradiance usually in W/m^2) in the area to predict the PV installation's power generation.

This data can have various sources. It can be acquired by interpolating the solar irradiance data from the nearest meteorological stations (Choudhary et al., 2020). This method lacks the ability to predict factors like the exact geometry of the installation or surrounding elements that can generate unexpected shades. It can also be obtained using simulation programs (like SolarEdge Designer or Archelios PRO) that can consider different geometries and surrounding elements but usually lack precision for the data on the incoming solar radiation. These two methods can also be combined to further improve the accuracy of the predicted data.

Another option is to log real data from the potential installation location and analyse it afterwards. This last option has the disadvantage of requiring a long time to gather enough data for the study but has the ability to account for local conditions. When this method is used, a solar radiation logger is used.

Professional data loggers usually cost several hundred euros at least. The most frequent practice is to store the data in internal memory, then export and process it after the study period is completed. In the 4.0 industry, IoT loggers with internet data transmission are being used too.

Thermopile pyranometers are the most used irradiation sensors used in the industry (Liang et at., 2012). These sensors give accurate data but are relatively expensive (usually several hundred euros). Photodiode-based pyranometers are being developed to decrease the cost of this type of sensor (Martínez et al., 2009; Rocha et al., 2021)). The price decrease usually comes with an increase in the uncertainty of the measurements. However, absolute accuracy is not always a requirement for the data, especially considering that the simulated data on solar irradiation might even be more uncertain.

Novia University of Applied Sciences is planning to install solar panels on the roof of the university building (Wolffskavägen 33, Vaasa, Finland), and a feasibility study will be conducted for the project. For that study, data on solar radiation will be necessary, and the preferred method of data acquisition is through real data logging over a period of time, expectedly, one year on distinct parts of the roof. This method is preferred since the geometry and external elements might considerably influence the PV system's performance and would be difficult to simulate. Additionally, transmission through the internet is preferred considering it is available. This thesis aims to develop a replicable solar radiation logger for the beforementioned study.

1.2 Aim and objectives

This thesis aims to design, build, and program a solar data logger for feasibility studies of residential and commercial scale PV installations. Requirements for the device are based on already available material and connectivity infrastructure. The usability of the device is also strongly considered. The specification supplied by the end-user were as follows:

- Based on an ESP32 microcontroller board.
- Data is logged through Wi-Fi with MQTT protocol.
- Data must be reliable, but not necessarily for meteorological purposes.
- Compact and encapsulated system.
- Resistant to all weather conditions.
- Good autonomy.
- Low-cost.

The following objectives are defined to achieve the aim:

- Study different sensor options and choose the most cost-effective one.
- Design a PCB that incorporates the ESP32 and all the necessary parts of the system.
- Program the ESP32 in a way that battery life is optimised.
- Generate a protective case for the system.

The beforementioned specifications are the minimal requirements for the device. Additional features can be appended during the development process as seen fit.

This thesis does not include the data reception mechanism's implementation or the data processing. Therefore, the validation of data measured over a long period is out of this project's scope.

1.3 Document structure

The information presented in this document is classified logically and does not strictly follow the chronological order of the development of the device. For instance, the hardware and software development was done parallelly in time, while these topics are clearly split in this document.

Section 2 seeks to introduce the reader to the world of data logging and commercial devices. Device development tendencies in the literature are also presented. Section 3 describes the device's general concept, enabling a detailed explanation of the hardware and software design and implementation from sections 4 and 5, respectively. Section 6 presents the case, which contains the system.

At this point, only how the device is made and how individual parts behave are described. Section 7 presents the system as a whole and its functionality. In Section 8, The device and this work are assessed and contrasted. Finally, in Section 9, this work is concluded.

2 Study background

Data loggers are devices that record and store any magnitude over time. These devices include a microcontroller, a storage unit (internal or external), a power supply (like a battery), and an appropriate sensor that quantifies the magnitude that is being recorded (OMEGA Engineering, 2018). A real-time clock can be part of the microcontroller unit or be included as a module but is necessary for timestamping the measurements. Data loggers are a type of data acquisition device which operate independently of a computer; hence they are perfect for operating in remote locations (Crystal, 2022).

Data loggers can have the sensors already incorporated or be modular and accept analog or digital signals from external sensors. The number of channels can also vary. Some companies like Pace Scientific offer a variety of sensors prepared to work with their own logging device. In contrast, other manufacturers like NOVUS Automation offer more versatile loggers with generic analog and digital channels.

Solar radiation loggers can be acquired as a standalone system composed of a single-channel logger and a radiation sensor (like the Electrocorder SR-1R Solar Irradiance Recorder from Acksen). Also, these loggers can be constructed by acquiring a solar radiation sensor and a compatible logger device.

The main difference between different solar radiation loggers is the type of sensor used. These can be thermopile or semiconductor pyranometers, reference photovoltaic cells, or even photovoltaic panels, depending on the data needed. For example, pyranometers can measure solar irradiance for meteorological purposes (Hukseflux Thermal Sensors, 2018), while reference PV cells are more suitable for monitoring the performance of PV systems (Atonometrics, 2013).

There is a clear interest in developing low-cost data loggers and irradiance sensors. Oliveira et al. (n.d.) published a user manual for building a cheap pyranometer based on a phototransistor as the primary sensor. The described device has a simple electronic system and needs an external power supply. The bill of materials indicates a total cost of around 50 $, although the cost of 3D printed elements was not realistically considered. The device could be modified into a logger by incorporating an external memory.

Rocha et al. (2021) proposed a photodiode-based solar logger that incorporates a data storage unit and a real-time monitoring system through MQTT protocol. The solution is not battery-powered, presumably because of the 5 Wh energy consumption. The device is more sophisticated than the pyranometer proposed by Oliveira et al. (n.d.) but for an estimated cost of 200 $.

Effendi et al. (2018) proposed a PV panel characterisation device that, by measuring voltage and current from the panel, could provide energy production patterns and therefore help assess potential areas for PV installations. This method only leads to the effective electrical

energy produced by the specific model, so the data would not fit meteorological purposes but provides enough information for the assessment. This approach is a clear example of a low cost and complexity achieved by specialisation. However, the presented device was not prepared for usage over extended periods of time.

Instead of developing solar loggers, some authors focus on generic low-cost solutions for solar radiation measurement, creating low-cost pyranometers or pyranometer-like sensors that could then be used for whatever purpose (including data logging).

Martínez et al. (2009) developed a sophisticated and market-competitive photodiode-based pyranometer similar to the one used in the device designed by Rocha et al. (2021). Vera et al. (2005) obtained good results building a less sophisticated but cheaper photodiode-based pyranometer.

Photodiodes seem to be the prime alternative to thermocouple pyranometers, but other options are also proved to be competent. Cruz-Colon et al. (2012) successfully approximated solar irradiance with mathematical models of PV panels and with open-circuit voltage and short-circuit current measurements under different irradiation conditions. Chen et al. (2012) relied on a photoelectric cell and successfully calculated the irradiance levels by measuring the cell's short-circuit current and temperature. Palo-Tejada et al. (2020) used a Peltier cell and artificial neural network to obtain the irradiance value by measuring the cell's open-circuit voltage and the cold face temperature.

3 General design

This section discusses the sensor selection, the working principle, and the device's general architecture. The sensor selection is crucial to this project and is thoroughly justified. The working principle and architecture are discussed to introduce the reader to the concept of this device and allow them to understand sections 4 and 5 better.

3.1 Solar irradiation sensor selection

In this section, the available options for solar irradiance measurement are discussed, and the selection of the sensor used in this project is justified.

3.1.1 Options

Quantification of solar irradiance for feasibility studies or PV panel performance assessments can be mainly done with pyranometers or reference PV cells. Pyranometers focus on quantifying the global horizontal irradiance (GHI), while reference cells are calibrated to quantify the irradiance available for photovoltaic energy production (Meydbray et al., 2012).

Pyranometers and similar instruments

As mentioned in Section 1.1, the most widely used GHI quantification instruments are thermopile pyranometers. These instruments consist, in essence, of a thermopile with a black-coated radiation absorber and a dome. They are passive sensors since the thermopile generates a voltage depending on the temperature of the absorber (Seebeck effect). Additional electronics and a power supply may be required to digitalise and transfer the data (Hukseflux Thermal Sensors, 2020).

Thermopile pyranometers are highly accurate devices because they usually have a flat response in the sunlight spectrum. Therefore, no corrections are required, and the irradiance can be measured with excellent linearity by knowing the equivalence between the irradiance and the thermopile voltage (Hukseflux Thermal Sensors, 2018; 2020). This accuracy and simplicity in signal conditioning make thermopile pyranometers a commercial but expensive solution (Tohsing et al., 2019).

Pyranometers can also be built using photodiodes (PD) or phototransistors (PT) instead of thermopiles. These sensors are also available commercially (Apogee Instruments, n.d.) but are commonly used for low-cost and non-profit purposes (Martínez et al., 2009; Tohsing et al., 2019).

Photodiodes can generate current proportional to the incident radiation in the same way as photovoltaic cells. The difference between photodiodes and PV cells is that the former

is optimised for light detection while the latter is optimised for energy conversion efficiency. Therefore, a better spectral response is expected from photodiodes (Tassell and Maule, 2002; University of Illinois at Urbana-Champaign, n.d.).

The spectral response of photodiodes ranges between ~300 nm and ~1100 nm (Tassell and Maule, 2002); therefore, about 80% of the energy can be captured (Apogee Instruments, n.d.). This behaviour leads to measurement errors that need to be compensated for and adds to the system's complexity. Also, a diffuser is required to match the angular response and be able to measure GHI (Martínez et al., 2009; Rocha et al., 2021).

Photodiodes generate current, but a conditioning circuit is essential to measure the magnitude correctly. Different measurement strategies and conditioning circuits lead to different results and should be chosen carefully (Pérez García, 2014).

Phototransistors work as BJTs, but the photoelectric effect does the base current injection. They have the same spectral bandwidth as photodiodes but need different condition circuits (Pérez García, 2014). Also, since the phototransistors' response is not linear, regression algorithms based on empirical data pools need to be used, adding another layer of complexity compared to photodiodes. Despite all the inconveniences, several authors like Oliveira et al. (n.d.) and Tohsing et al. (2019) have shown low-cost pyranometers with good results.

Probably the cheapest device that allows solar radiation quantification is a light-dependent resistor (LDR). As their name suggests, LDRs are passive components whose resistance value varies with the incident electromagnetic radiation. The spectral response of an LDR depends on the semiconductor used for its fabrication. The most used semiconductor is CdS since it has a high spectral response to visible light (Pérez García, 2014).

De Barros et al. (2018) and de Sousa et al. (2018) have created irradiance sensors based on LDRs calibrated to work as similarly as possible to a pyranometer. The main interest for LDRs is their low price. However, this sensor type has several disadvantages, such as a narrow spectral response and non-linearity.

According to de Barros et al. (2018), 95% of solar energy comes from radiation between 400 nm and 1200 nm of wavelength. But the spectral response of CdS LDRs ranges, non-uniformly, between 300 nm and 900 nm (de Barros et al., 2018; RS Components, 1997), inducing error in the measurements. The non-linearity can be corrected with mathematical regression models based on data pools which provide a relationship between the global irradiance and the voltage response of the sensors.

Reference PV cells and similar

Reference PV cells are, in essence, photovoltaic cells whose current is conditioned, measured, and translated to available irradiance for the PV cell (instead of broadband

irradiance). This way, these sensors are more suitable for measuring PV efficiency than solar radiometric measurements (Meydbray et al., 2012).

Reference PV cells are usually used as a supportive sensor to pyranometers considering they have several issues like their behavioural dependence on the materials and coating used. They can perform better than pyranometers if used to monitor the behaviour of a PV panel made with the same material and coating (Hukseflux Thermal Sensors, 2017; Meydbray et al., 2012b).

To evaluate potential solar energy areas, using PV panels can also provide enough information, even without knowing the actual irradiance (Effendi et al., 2018). This method is most possibly not widespread since arriving to conclusions only knowing the produced energy might be complex in some cases. In contrast, Cruz-Colon et al. (2012) and Chen et al. (2012) designed sensors based on a PV panel by mathematically approximating the irradiance based on the I-V characteristics of the PV panels.

3.1.2 Selection

The following aspects are going to be considered to select the sensor that is going to be used for this project:

- Availability: whether the sensor can be found commercially or needs to be fabricated as a custom-made device.
- Measured magnitude: the magnitude that the sensor is capable of measuring.
- Accuracy: accuracy in the sense of absence of error or uncertainty.
- Usual cost: the typical price of the commercial product or the primary sensor (excluding conditioning circuit and peripherals) in the case of custom-made sensors.
- Complexity of development: how difficult it is to obtain the desired magnitude from the signal generated by the sensor element in the case of custom-made sensors.

Contrasting all the information, for the scenario described in Section 1.1, using a PV panel to monitor the generated power suffices the information needs for the feasibility study. Moreover, PV panels are relatively cheap, and the complexity of the electronics required to measure the power production of a PV panel is low.

Table 1 shows the beforementioned aspects for each type of sensor discussed in Section 3.1.1. The typical cost of single electronic components was contrasted in the catalogue of Mouser Electronics.

Contrasting all the information, for the scenario described in Section 1.1, using a PV panel to monitor the generated power suffices the information needs for the feasibility study. Moreover, PV panels are relatively cheap, and the complexity of the electronics required to measure the power production of a PV panel is low.

Table 1: Solar sensor comparison table

Sensor	Availability	Measured magnitude	Accuracy	Usual cost (in euros)	Complexity of development
Thermopile pyr.*	CM**. Custom-made not recommended	GHI with a flat spectral response	Highest	>100	N/A
PD-based pyr.	CM and custom-made options	GHI after compensating for SBW	High	>100 for CM <20 for a PD	Medium-low
PT-based pyr.	Custom-made only	GHI after compensating for SBW and non-linearity	Medium-high	<20 for a PT	Medium-high
LDR-based sensor	Custom-made only	GHI after compensating for SBW and non-linearity	Medium	1~2	High
Reference PV cell	CM. Custom-made not recommended	Irradiance available for PV energy conversion	High[1]	>100	N/A
PV panel[2]	Custom-made only	PV power generated	N/A	~20 for 5 W panels	Low

*Pyranometer | **Commercial model

If the power production of a solar panel is known, the relative production compared to its rated power can be an indicator of the ideality of the meteorological conditions for solar power generation. However, the relative production of different solar panels can differ in the same meteorological conditions if their spectral response is not identical.

Additionally, if several loggers are used for the same study, relative performances can be evaluated between solar panels. This way, for example, the best-performing solar panel can indicate the best location for solar panel installation.

Although having only a PV panel as a sensor could provide enough information, having an optional pyranometer as a supportive sensor can be convenient. Knowing the correlation between the power production and GHI for a particular PV panel, if the sensor is replicated with the same solar panel, the data can be extrapolated, making it possible to determine the GHI based on the power generation.

3.2 Working principle

The data logger is going to be based on an ESP32 system on chip (SoC), given that it has a built-in Wi-Fi module, a real-time clock (RTC), and all necessary peripherals such as digital and analog inputs and outputs (Espressif Systems, 2022). The device is battery-powered and has a solar panel as the main sensor with an optional input for a pyranometer. Besides acting as a sensor, the PV panel also charges the battery, making the system practically autonomous. However, even though the battery can be recharged with the PV panel, power efficiency help reduce cycling, extending battery life.

[1] The accuracy is high but only if used for predictions or assessment of PV efficiency of the same type (material and coating) as the sensor.
[2] This refers to a PV panel with a current and voltage sensor to measure the power generated.

Additionally, three temperature sensors provide essential environmental information such as the air and PV cell temperature to correlate these values with the irradiance; and the battery's temperature to prevent charging or discharging the battery in extreme heat or cold.

The data be stored only temporarily on the device. Several measurements are grouped in small packs (measurements over one or two hours every five or ten minutes, for example) and automatically transmitted over MQTT protocol to a broker every time a pack is ready. This way, an external non-volatile storage unit (NVS) is not required. Also, sending data packs instead of individual measurements minimizes the time the system is connected to Wi-Fi, consequently reducing energy consumption.

Assuming Wi-Fi connectivity is available, the system can obtain information about sunrise and sunset times. This way, data logging can be stopped during the night, further improving power efficiency. Also, the system time can be updated through a Network Time Protocol (NTP) server to compensate for the cumulative error of the RTC.

3.3 Architecture

The general hardware schematic that implements what was described in Section 3.2 can be seen in Figure 1.

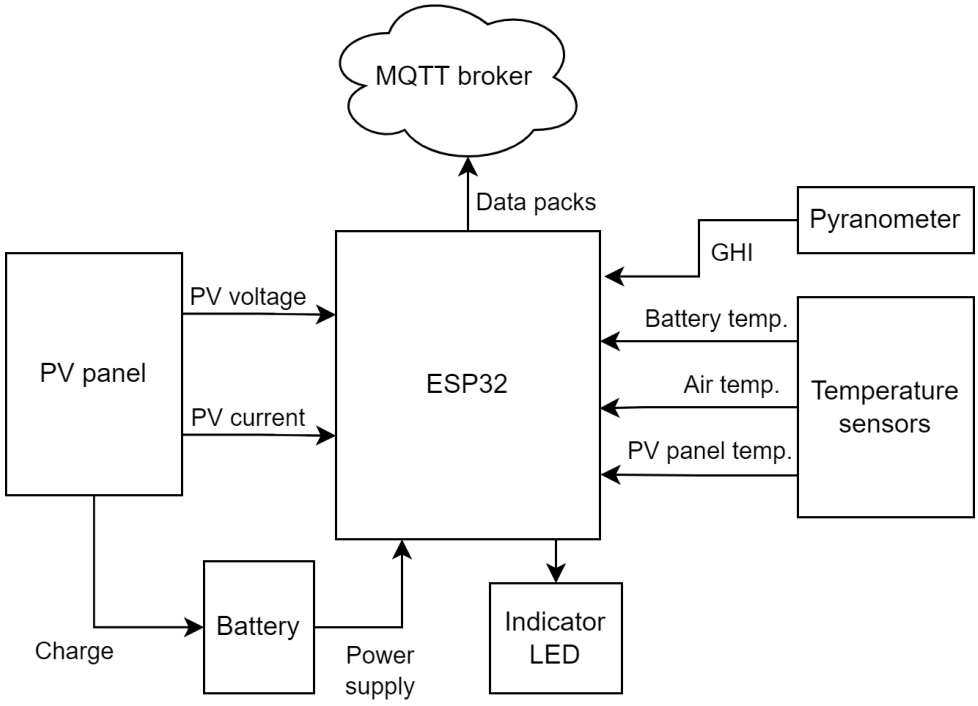

Figure 1: Block diagram of the general hardware for the solar data logger

The ESP32 is the system's centre, managing all inputs and outputs. Inputs are measurements and the power supply. Outputs are an indicator LED that allows general debugging of the system and the data to the MQTT broker.

In the block diagram above, the dual function of the PV panel is clear. The panel is used as a sensor (measuring its voltage and current output) and as a supply to recharge the battery. The temperature sensors and the optional pyranometer provide additional information about the environment.

Figure 1 only shows the main components and their general relationship. All the intermediate components and auxiliary electronics are discussed in Section 4.

4 Hardware design and implementation

In this section, the final hardware is discussed. First, the design without specific components is presented. Then, the selection and justification for each required component are addressed. Finally, the implementation of the hardware on a printed circuit board (PCB) is reviewed.

4.1 Basic hardware design

The hardware must incorporate and successfully interconnect all the components shown in Figure 1. The hardware can be classified into two generic categories. The first one is power management which includes all the components required to adapt the battery voltage to a steady voltage supply for all the main components and to charge the battery. The second category is signal conditioning, which includes all the components to adapt the signals from the sensors for the ESP32.

In Figure 2, the proposed power management circuit for the solar logger can be seen. The red connections are feeding paths, and the blue ones are the return paths.

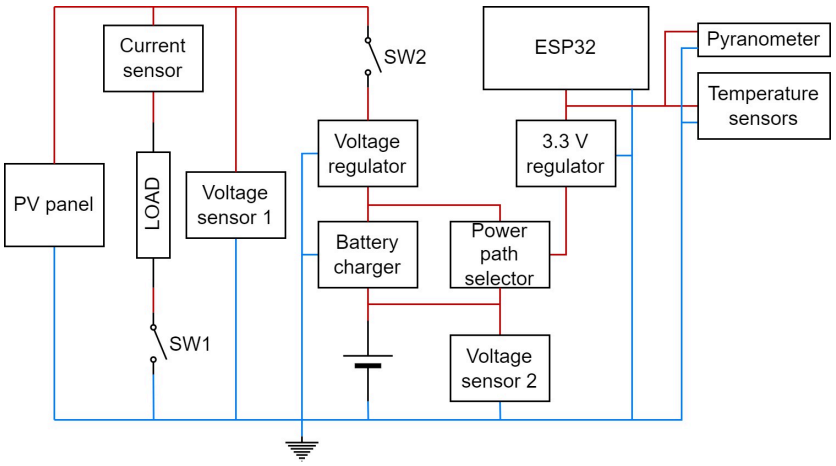

Figure 2: Block diagram of the power management circuit for the solar logger

Considering that a PV panel can be modelled as a current source, a load needs to be connected to measure the generated current and power. A current sensor (in series with the beforementioned load) and a voltage sensor (in parallel with the beforementioned load) are needed to quantify the power generated.

The load could be permanently connected to the PV panel, but it would decrease the charging efficiency since it would dissipate power that otherwise could be used for the charging. Therefore, a switch is needed to disconnect the load.

Since the ESP32 modules use a 3.3 V supply, a 3.3 V regulator is needed to adjust the oscillating battery voltage to a steady 3.3 V. As for the charging of the battery, a battery charger that can control the charging current is essential. A voltage regulator that can

adjust the voltage of the solar panel to the value required by the beforementioned charger is also required.

While the battery is charging, the ESP32 module and additional components cannot be powered by the battery. So a power path selector is required to feed the 3.3 V regulator not from the battery but from the regulated PV voltage.

A voltage sensor to measure the battery voltage can provide helpful information to determine when charging is needed. And to discontinue the charging process, the PV panel must be disconnected. Therefore, a switch is required before the voltage regulator.

For signal conditioning, digital interfaces are better suited to transfer reliable signals to the ESP32 microcontroller for two main reasons. First, analog signals are more susceptible to noise and transmission problems in general (Rao, 2021). Second, the built-in analog to digital converters (ADC) of the ESP32 is known to have low accuracy with ± 60 mV in the 150~2450 mV range (Espressif Systems, 2022) and be unsuitable for precise measurements in consequence (Spiess, 2020). Therefore, having digital sensors or a digital interface for each of the sensors would be ideal.

4.2 Component selection

In this section, all the subsections are dedicated to the discussion and justification for the parts selected. For all individual electronic components, surface-mount technology (SMT) is preferred over through-hole technology (THT) to save space and manufacturing time (reducing the drilling process) for the PCB. Only packages and sizes that can be hand-soldered among the SMT components are considered.

4.2.1 Controller

The ESP32 SoC can be acquired as a component or as part of a development board. Working with a standalone component can be more efficient in design and simplicity. However, a development board already incorporates essential components like a 3.3 V regulator and a USB interface for programming.

The Olimex ESP32-Devkit-LiPo (Rev. C) is used for this project because it is a model already available in the Energy Technology Laboratory and has peripherals for battery-powered applications. Other companies also offer boards optimised for battery-powered applications. However, Olimex has designed well and achieved a very low quiescent current consumption (Spiess, 2021). In Figure 3, the power supply solution of the Olimex board can be seen.

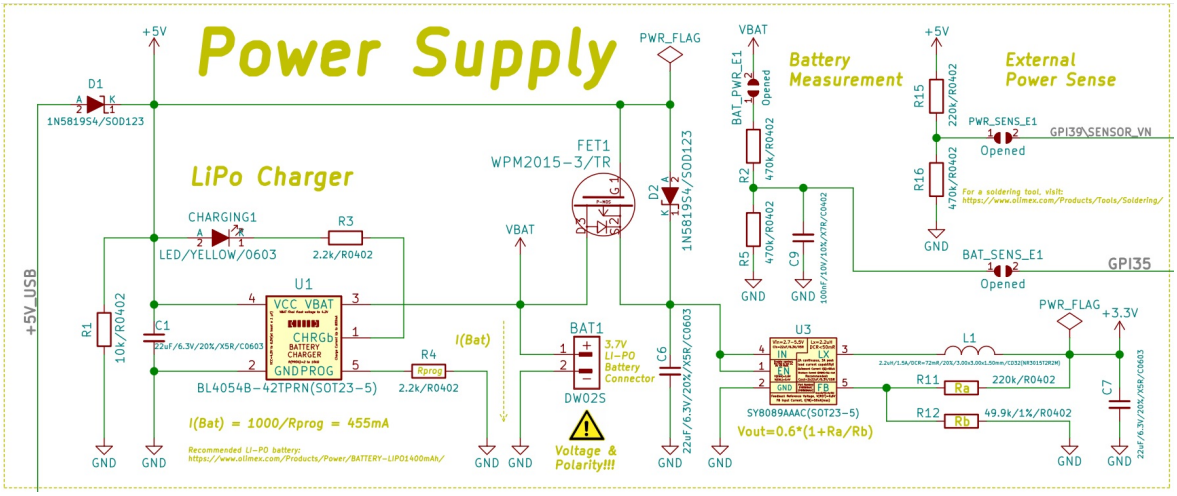

Figure 3: Schematic of the power supply solution of the ESP32-Devkit-LiPo Rev. C. Adapted from DanKoloff and TsvetanUsunov (2020)

The ESP32-Devkit-LiPo board incorporates an SY8089AAAC switching regulator configures for 3.3 V output. This switching regulator accepts input voltages up to 6 V, has high efficiency (over 92% for 3.3 V output), and consumes a decently low 55 µA (typical) quiescent current (Silergy Corp, n.d.). However, better regulators do exist even from the same company.

The board also has a BL4054B-42TPRN Li-ion battery charger configured to charge at a constant 455 mA. The IC accepts input voltages up to 10 V and has many features, such as a charging status indicator, automatic termination ending at 1/10th of the charging current, low voltage trickle charging, and thermal regulation (Shanghai Belling, 2009).

The board included a power path using a WPM2015-3/TR P-channel enhancement MOSFET which cuts the battery output if a power supply is connected with a higher voltage than the battery and enters saturation when the power supply is disconnected. Considering that there is a 22 µF capacitor at the input of the voltage regulator, instant changes between the battery and an external power supply are possible without interrupting the power supply to the ESP32 or having brownouts.

Some minor yet useful features include battery voltage sensing and an external power supply sensing, both done with a voltage divider connected to GPI35 and GPI39, respectively, through a jumper. Connecting the respective jumpers allows the voltages to be measured with the built-in ADC, although with low accuracy, as mentioned in Section 4.1.

4.2.2 Solar panel

The factors taken into account for the PV panel selection are the output power and the number of PV cells in series. The output power should be enough to power the solar logger and charge the battery. Rounding the charging and power consumption of the ES32 board

to 500 mA at around 4 V (for a Li-ion battery), 2 W should satisfy the needs. However, power ratings for solar panels are done in standard test conditions (irradiation of 1000 W/m^2, at 25 ˚C, with an AM1.5 spectrum) (Villalva et al., 2009), which are rarely met, especially the irradiance levels. 4 to 5 W solar panels should guarantee a decent charge at irradiances of 500 W/m^2.

The number of PV cells in series directly indicates the voltage levels since every cell adds about 0.5 V at the maximum power point (Honsberg and Bowden, 2019b). A low number of cells in series translates into a low voltage output, while a high number means higher voltages. Too high of a voltage is not desired because it needs to be regulated down to around 5 V and voltage regulators tend to increase in price with their input voltage range. Too low of a voltage (close to 5 V) would mean oscillating above and below 5 V, depending on the current consumption. Therefore, a step-up/step-down converter is needed (which is more expensive than a step-down converter). Usual configurations are 36, 60, and 72 cells, but there are unique designs with fewer cells. For this project, a 36-cell panel is well suited, and the following models are tested:

- Enjoy Solar - Eco Line ES5P36: 5 W capable with 36 polycrystalline silicon cells.
- Offgridtec - ACM156: 5 W capable with 36 monocrystalline silicon cells.

4.2.3 Measurement load

A load should be connected to measure the current and voltage of the PV panel. However, this load's value directly influences the PV panel's operating point along its I-V curve. The most interesting operating point to be determined is the maximum power point (MPP), and it can only be achieved with the optimal load connected (Honsberg and Bowden, 2019c).

To test how much the value of the optimal load varies with irradiance and cell temperature, a Simulink model of the PV panel with a load has been created (Figure 4).

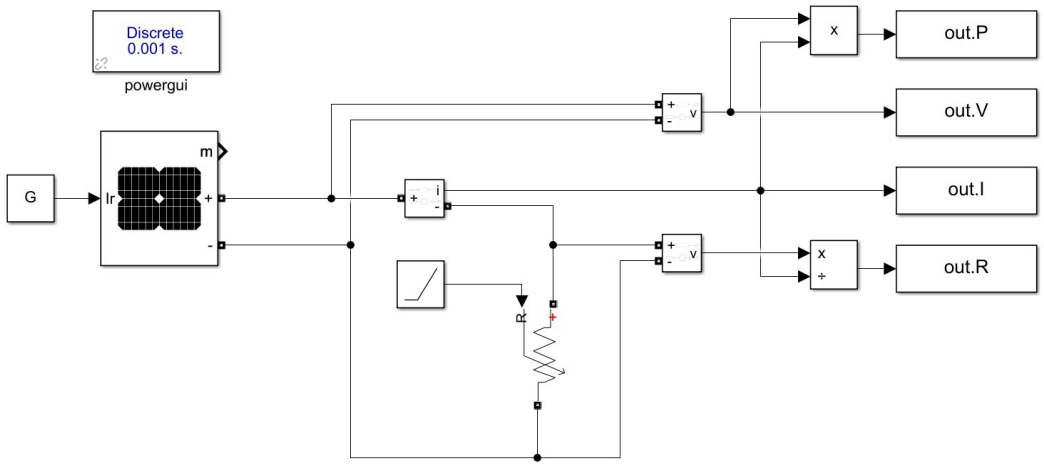

Figure 4: Simulink model of a PV panel with a variable load

The model includes a PV panel block that generates the single diode model based on the following parameters:

- Cells per module
- Open-circuit voltage
- Short-circuit current
- Voltage at MPP
- Current at MPP
- Temperature coefficient of the open-circuit voltage
- Temperature coefficient of the short-circuit current

All the beforementioned parameters are known for the Eco Line ES5P36 but not the temperature coefficients of the ACM156 model. Since all known parameters are very similar for the two panels, simulations are only done for the Eco Line ES5P36 model, assuming that the results would be similar for the other panel.

In the Simulink model, the irradiance and temperature of the PV panel are inputs. The value of the resistor increases 1000Ω/s starting at 1 Ω. The model is configured as a discrete system with a time step of 1 ms, and the simulation runs for 1 second, sweeping the load from 1 to 1001 Ω every 1 Ω. The simulation returns the voltage, current, and power generated by the PV panel as well as the resistance for each measurement.

A MATLAB script executes the simulation for an array of irradiances and temperatures and computes the maximum power for each combination of conditions, determining the optimal load. The results for the Eco Line ES5P36 panel can be seen in Table 2.

Table 2: Simulated maximum power (orange) and optimal load (blue) values for an Eco Line ES5P36 PV panel under different irradiance and cell temperature conditions

T [°C] → / G [W/m²] ↓	-20	-10	0	10	20	30	40	50	60	70	80
100	0.573 745	0.550 711	0.528 678	0.505 646	0.482 614	0.458 582	0.435 550	0.408 554	0.377 439	0.363 456	0.326 481
200	1.169 381	1.125 364	1.081 347	1.037 331	0.992 317	0.946 301	0.900 285	0.854 269	0.793 281	0.747 219	0.713 229
300	1.772 267	1.707 245	1.642 234	1.576 224	1.509 214	1.442 203	1.374 193	1.306 184	1.235 179	1.126 146	1.093 147
400	2.439 265	2.291 185	2.205 177	2.118 170	2.030 162	1.942 154	1.852 147	1.762 139	1.671 132	1.536 142	1.468 108
500	3.206 263	2.875 149	2.768 143	2.661 136	2.552 130	2.442 124	2.332 118	2.220 112	2.107 106	1.968 109	1.837 85
600	4.070 261	3.458 124	3.332 119	3.204 114	3.074 109	2.943 104	2.811 99	2.678 94	2.544 89	2.397 89	2.200 70
700	5.029 259	4.041 107	3.893 102	3.745 98	3.595 94	3.443 89	3.290 85	3.135 81	2.980 77	2.818 75	2.565 66
800	6.081 257	4.621 94	4.454 90	4.285 86	4.114 82	3.941 78	3.767 75	3.592 71	3.414 67	3.235 64	2.954 66
900	7.223 255	5.208 90	5.012 80	4.822 76	4.631 73	4.438 70	4.242 66	4.046 63	3.848 60	3.649 57	3.365 61
1000	8.453 253	5.827 90	5.567 72	5.358 69	5.146 66	4.932 63	4.717 60	4.499 57	4.279 54	4.058 51	3.775 54

The simulation shows that the maximum power generation increases with irradiance and decreases with cell temperature. The temperature ranges from -20 to 80 ˚C because the cell temperature can be close to the ambient temperature for low irradiances or be several tens of degrees Celsius above for high irradiances (Honsberg and Bowden, 2019d).

The optimal resistance value varies with both irradiance and temperature but strongly depends on the irradiance. Conditions outside the ones considered for the simulation would be rare or irrelevant (like irradiances below 100 W/m^2). It can be concluded then that the load used for the PV power measurement must be variable in the range of 50 to 750 Ω to track the MPP.

In essence, to measure the power production at the MPP, the P-V curve of the PV panel must be acquired for the irradiance and temperature at the measurement time. Obtaining the I-V also results in the P-V curve and is known as the I-V characterisation of a PV panel.

Usually, the I-V characterisation aims to generate the I-V curve from open-circuit (maximum voltage) to short-circuit (maximum current) conditions. However, for this project, obtaining only the part of the I-V curve where the MPP can be found is enough.

Several techniques discussed in the literature allow the I-V characterisation of PV panels. Duran et al. (2008) overview most of the techniques commonly used. Honsberg and Bowden (2019a) suggest that using voltage sources that can sink current is the most common method, but it requires sophisticated electronics. For this project, the simplicity, the speed, and the ability to partially characterise the PV panel are key factors to consider.

The simplest method to vary the load is to connect different resistors to the PV panel. Sharko et al. (2011) changed the resistors manually, but it can also be done automatically with relays (Duran et al., 2008). In any case, the resolution strictly depends on how many resistors are used (which implies a large space requirement for high resolution), and the acquisition speed is slow. For these reasons, this method is unsuitable for this project.

A capacitive load can increase the speed to the order of hundreds of milliseconds (Chang et al., 2018). The capacitor sweeps in a continuous spectrum, and the resolution of the I-V curve depends on the measurement device's speed since the sweep time depends on the capacitor's size. This is not a convenient method for this project because partial sweeps are impossible (Duran et al., 2008).

DC-DC converters provide a very reliable and fast characterising (Duran et al., 2008). However, the complexity of the electronics required for both the converter and the control system to adjust the duty cycle makes this option not very attractive for this project.

A MOSFET-based electronic load is the most suitable option for the scenario under discussion. This method has many variants, but the working principle is to operate a MOSFET with a gate-to-source voltage (V_{GS}) close to the threshold voltage to regulate the current flow, varying this way the equivalent resistance. Kuai and Yuvarajan (2006) show

how using a sinewave as the gate signal can achieve high-speed measurements (40 ms for a whole cycle). Forero et al. (2006) obtained the entire I-V curve in less than 5 seconds, and Sahbel et al. (2013) in 6 seconds. The proposed electronic load can be seen in Figure 5.

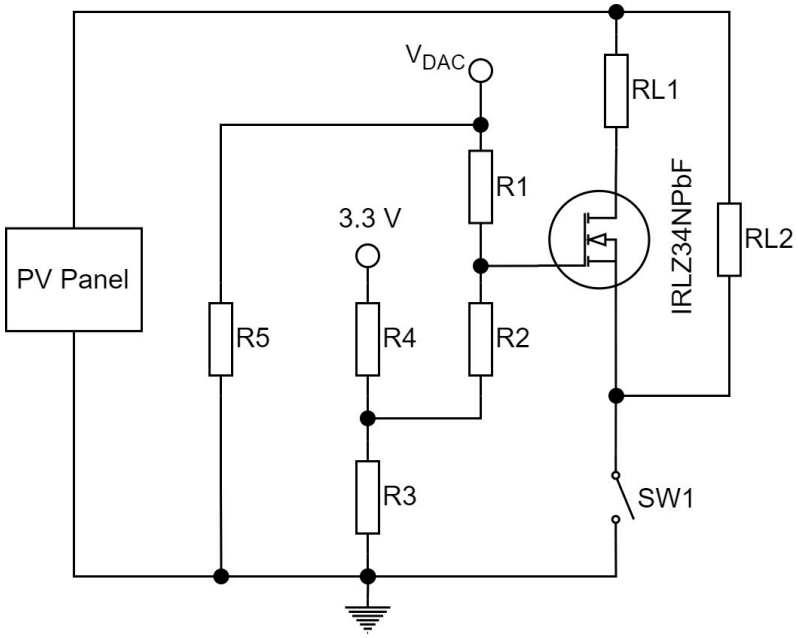

Figure 5: Proposed MOSFET-based variable electronic load

The electronic load is composed of RL1, RL2, and the MOSFET. With only one MOSFET, the load resistance values would ideally range between zero and infinity. But, since the only region of interest is between 50 and 750 Ω, the load value should be restricted to this range to increase the accuracy of the MPP measurement (having a fixed resolution). Moreover, reducing the upper limit to about 600 Ω would only compromise low temperature and low irradiance scenarios, which are generally not very interesting for power generation (because of the low irradiance condition). The narrower the range, the better the accuracy. On the other hand, the lower limit is worth reducing to about 30 Ω so that during the sweep, the MPP can have a context for higher irradiance values.

RL2 is added in parallel to the MOSFET to restrict the load range, forcing an upper resistance limit. RL1 is added in series with the MOSFET to force a lower limit. The upper limit is the value of RL2, and the lower limit is the value of RL1 in parallel with RL2. RL2 is chosen to be 620 Ω, and RL1, 33 Ω. Therefore, the load can vary between 31 and 620 Ω.

RL1 and RL2 must be power resistors since they have to withstand the power production of the PV panel. In the worst-case scenario, they have to withstand the rated power of 5 W (ignoring the rare cases with higher production from Table 2). So, if both RL1 and RL2 are 5 W resistors, there should be no problem since none of the components has to withstand the burden alone. The selected resistors are the ROX5SSJ33R and the ROX5SSJ620R.

The selected MOSFET is the IRLZ34NPbF model. This device is suited for power applications up to 30 A at 25 ˚C, but the most interesting features are its low threshold voltage and a

sufficiently low drain current increase with the gate-to-source voltage (Infineon Technologies, n.d.).

The idea is to control the gate voltage of the MOSFET with the 8-bit digital to analog converter (DAC) output of the ESP32, which can theoretically range between 0 and 3.3 V (Espressif Systems, 2022). The real output range of the DAC has been experimentally measured and resulted in [0.07, 3.2] V.

The MOSFET's resistance does not vary along the DAC's output range. The actual range of V_{GS} that translates into the full load range has been empirically measured to increase the precision of the control. The test circuit used can be seen in Figure 6.

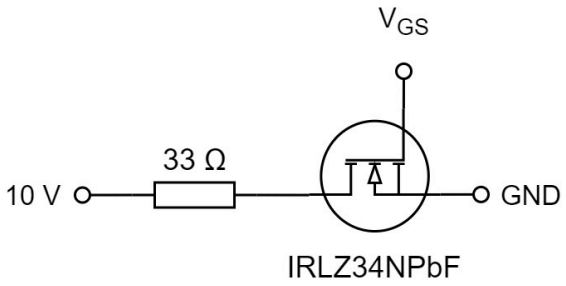

Figure 6: Test circuit for V_{GS} limits for a MOSFET

A voltage source was used to bias the MOSFET with arbitrary 10 V, and V_{GS} was generated with the DAC of the ESP32. The voltage at the MOSFET's drain was measured. The drain voltage was practically 10 V when the MOSFET was not conducting. The drain voltage was practically 0 V when the MOSFET was completely conducting. The MOSFET acted as an open circuit until V_{GS} reached around 1.6 V and started acting as a short circuit after reaching around 2.4 V.

To fully take advantage of the DAC of the ESP32, its range of [0.07, 3.2] V must be reshaped to [1.6, 2.4] V. Using an operational amplifier as a non-inverting amplifier with an offset would be the most straightforward solution. But, since the range [1.6, 2.4] V is included in [0.07, 3.2] V, it is possible to achieve the same effect using only resistors connected as R1 to R4 in Figure 5, given the high gate impedance of MOSFETs. Using only resistors reduces the system's overall cost and complexity.

The idea behind the circuit is to use the 3.3 V output of the ESP32 and a voltage divider (R3 and R4) to generate and offset and to use another voltage divider (R1 and R2) to amplify the DAC output by a factor lower than the unity. In reality, the voltage dividers interact, so the circuit must be solved as a system to calculate the values of the four resistors that generate the desired offset and amplification.

One combination of E12 series resistors that achieves a theoretical range of [1.55, 2.39] V (which is close enough to the target range of [1.6, 2.4] V) is R1 = 560 kΩ, R2 = 180 kΩ, R3 = 68 kΩ, and R4 = 39 kΩ. High resistance values have the advantage of reducing current consumption. The calculations can be found in Appendix 1.

The circuit from Figure 5 has been built to test the system, but with a power supply instead of the PV panel and with the DAC voltage simulated by a second power supply. The easiest way to test the system would be to measure V_{GS} with an oscilloscope for the entire range of the DAC's output. However, the resistance values are close enough to the available oscilloscope's input impedance (1 MΩ) to alter the measurements. Therefore, manual measurements were performed with a multimeter on the circuit shown in Figure 7.

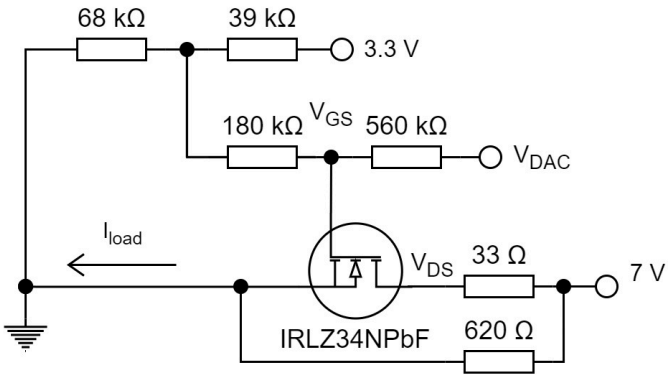

V_{DAC} [V]	V_{GS} [V]	I_{LOAD} [mA]	R_{LOAD} [Ω]*	V_{DS} [V]
0.00	1.55	11	636	6.98
0.50	1.68	12	583	6.95
1.00	1.82	18	389	6.68
1.50	1.95	55	127	5.20
2.00	2.05	150	46.7	0.447
2.50	2.20	210	33.3	0.07
3.20	2.38	213	32.9	0.04

* Calculated as $R_{LOAD} = 7/I_{LOAD} \cdot 1000$

Figure 7: Test circuit for the electronic load controlled by the ESP32 (left) and the test results (right)

Results show that the electronic load works quite close to the theoretical values. The range of V_{GS} is practically identical to the theoretical one. The range of the load resistance is close to the target; however, the results might be influenced by the accuracy of the load current values. By observing V_{DS}, it can be seen that the MOSFET operates from practically open-circuit to practically short-circuit conditions. It must be noted that the evolution of R_{LOAD} is not linear with V_{DAC} or V_{GS}.

In Figure 5, R5 is a strong pull-down resistor that is necessary to keep V_{DAC} close to 0 V when the DAC is not active. The lower the value, the stronger the pull, but the current consumption increases when the DAC is in use. A 4.7 kΩ resistor pulls V_{DAC} down to 25±5 mV with a peak current consumption of about 600 mA when the DAC outputs maximum voltage. A 2.7 kΩ resistor pulls V_{DAC} down to 15±5 mV with a peak current consumption of about 1100 mA. The latter option is preferred since the active phase of the DAC is limited to the time the I-V characterisation of the PV panel requires, and the current consumption increase is not critical in this case.

4.2.4 Buck converter

The voltage has to be regulated to 5 V to use the power generated by the PV panel, which is a safe voltage for both the battery charger and the 3.3 V regulator from the ESP32-Devkit-LiPo board can use.

36-cell PV panels have open-circuit voltages of around 22 V. Any buck converter with an absolute maximum rating for the input voltage higher than 24 V (a typical value) suffices the voltage limitations. To power both the ESP32 module and the battery charger, the

minimum current output capability of the converter should be around 1 A (Espressif recommends 500 mA or more for the ESP32 SoC, and the battery charger is configured to charge at 455 mA).

The selected buck converter is the V7805-1500. This IC complies with all the requirements and has the advantage over other converters that it does not require external components besides two capacitors (acting as an input and an output filter). Most buck converter ICs require external inductors and resistors to program the feedback value.

The capacitors recommended by the manufacturer are one 10µF/25V and one 22µF/16V ceramic capacitor. The selected models are the TMK316AB7106KL-T and the EMK316BJ226KL-T model, respectively.

4.2.5 Battery

Most Li-ion or LiPo batteries could suffice the needs of the system. 18650 Li-ion cells would be well-suitable, for example. The only capacity limitation is that, in cold regions, the battery should last the whole winter when the average temperature is below 0˚C (Li-ion and LiPo batteries cannot be charged in temperatures below zero). During warmer periods, the solar panel should be able to recharge the battery whenever needed.

The selected battery is the JA-803450P LiPo model, which is the one recommended by Olimex for their ESP32-Devkit-LiPo board. However, changing the battery is possible and does not require hardware modifications.

4.2.6 Temperature sensor

Three temperature sensors are needed in total. There are many options on the market, but the DS18B20 model was chosen because they were already available in the Energy Technology Laboratory.

This temperature sensor already has a built-in digital interface (1-Wire) and is prepared to incorporate many sensors over the same communication bus (Maxim Integrated, 2019). The DS18B20 IC only requires a 4.7 kΩ pull-up resistor for the 1-Wire bus line to work.

4.2.7 Current sensor

There are two types of current measurement techniques: using shunt resistors or based on the Hall effect. Resistive measurements are usually more accurate over a wide range of currents and have lower temperature dependency. On the other hand, magnetic sensors offer isolation from the circuit and do not introduce voltage drops in the circuit, unlike resistive ones. (Keim, 2015; GlobalSpec, 2020).

Since the lack of isolation and minor voltage drops are not problems for this project, resistive sensors seem better suited. Building a current sensor from scratch is not very difficult: it mainly requires a shunt resistor and an operational amplifier. However, plenty of current sensing ICs are easier to implement, and some even have a digital interface.

The INA219 model was chosen because of its popularity and availability in the Energy Technology Laboratory. This IC incorporates bus and shunt voltage measurement capability. Therefore, it can be used to measure both the PV voltage and PV current. The chip also incorporates an I^2C digital interface for communication (Texas Instruments Incorporated, 2015).

The INA219 IC requires very few external components to work. The necessary components are a shunt resistor, whose value needs to be selected according to the measurement range; two strong pull-up resistors for the I^2C bus lines; and a decoupling capacitor (Texas Instruments Incorporated, 2015).

To size the shunt resistor, the current to be measured and the voltage range of the INA219 must be considered. The maximum expected current from the PV panel is about 300 mA. The INA219 chip has four shunt voltage measurement ranges, but the precision of the measurement (10 μV) is not altered. The narrowest range ([-40, 40] mV) is chosen to minimize the influence of the shunt resistor in the measurement. By choosing a 100 mΩ resistor, currents up to 400 mA can be measured, which leaves a large margin for the expected 300 mA.

When choosing a shunt resistor, the temperature is an important parameter besides the resistance value and power rating, but only if high currents are expected. High currents can make the component reach high temperatures and alter its resistance. This phenomenon is not a concern for the application under discussion because the maximum power dissipation expected is 30 mW over 100 mΩ.

4.2.8 Pyranometer and required peripherals

Selecting a pyranometer can be difficult (Hukseflux Thermal Sensors, 2018a). But the selection process was skipped because the SR05-D1A3 model was already available in the Energy Technology Laboratory. This pyranometer is classified as a spectrally flat Class C (second class) according to the ISO 9060:2018 classification (Hukseflux Thermal Sensors, 2021).

It has an analog output as well as a Modbus over RS-485 interface. The latter option is more attractive for all the reasons discussed in Section 4.1, but it requires an RS-485 transceiver to adapt the RS-485 signal to TTL levels that the ESP32 can read and write.

The selected transceiver is the MAX3483AEASA+ model because it uses a 3.3 V supply, can operate in negative temperatures up to -40 ˚C, has a low data rate (no fast communication is required), and is one of the few models still in stock at electronics suppliers.

The transceiver requires only pull-up and pull-down resistors to work correctly. The RE, RO, and DI pins require a pull-up to 3.3 V. The DE pin can have either a pull-up or a pull-down, but it is more intuitive to be pulled down because then the default state of the transceiver would be to either transmit or receive.

The pyranometer needs to be powered with a voltage between 5 and 30 V. That means a boost converter must increase 3.3 V to at least 5 V. The current requirements are low since the pyranometer is rated to use 75 mW with a 12 V supply.

The converter selected is the MAX8569AEUT+T because it complies with all the requirements at a relatively low price. This IC requires an external inductor, two capacitors, and two resistors to work.

The manufacturer recommends a 10 µH inductor for general applications, so the 744042100 model was selected. The input capacitor is chosen to be only 10 µF since no input voltage variation is expected. The output capacitor is chosen to be 22 µF as recommended in the datasheet. The two resistors must be chosen to set the output voltage to the desired value. Any output voltage between 5 and 5.5 V is adequate, so the E12 series resistors chosen are 390 and 120 kΩ setting a theoretical output of 5.22 V.

4.2.9 Solid-state switches

The solid-state switches can be implemented with BJTs or MOSFETs. MOSFETs are chosen for this project because they consume less current when driven and can be easier to drive (Hlapisi, 2021).

Both P-channel and N-channel MOSFETs are needed. N-channel MOSFETs are used as low-side switches and to drive P-channel MOSFETs. P-channel MOSFETs are used as high-side switches. The models selected are the DMN3150L-7 and the DMP3130LQ-7. These transistors offer a very low threshold voltage and very fast switching. They can tolerate much more current than required but are inexpensive enough to avoid selecting a specific MOSFET with adequate current capabilities for each application.

4.2.10 Indicator LED

An RGB LED was chosen because it allows the use of colour codes for errors or general debugging. The specific model selected is the OSTA5131A-C because it was already available in the Energy Technology Laboratory.

Three resistors need to be selected to properly use the device, one for each colour. The resistors limit the current for each LED. The current value can be fine-tuned for each of them to provide the same luminous intensity for the same voltage, but this is a tedious process and unnecessary for this project. Instead, it was empirically tested that 56 Ω for the red LED and 12 Ω for the green and blue LEDs give good enough results.

4.2.11 General purpose resistors and capacitors

SMD resistors and capacitors are usually bought in so-called catalogues, which include a fair amount of various values of components of the same package. For this project, a thick film chip resistors catalogue of the RTT06 series and a ceramic capacitor sample kit (EIA 1206) was available. Some additional capacitors complemented the EIA 1206 kit. The additional models were the C1206C226M8PACTU (22µF/10V) and the 12062C103KAT2A (10nF/200V).

4.2.12 Connectors

For general connections, standard 0.100" pitch pin headers are used. A 3.5 mm pitch screw terminal is used to connect the PV panel, specifically item number 19963 by 4UCON TECHNOLOGY INC.

4.3 Final hardware design

Once all the components have been selected, the hardware schematic can be prepared. There are still some gaps in the design to be filled. These gaps are the specific designs of the solid-state switched and some modifications to the ESP32-Devkit-LiPo.

From Figure 2, SW1 is a low-side switch and it must be implemented with an N-channel MOSFET. This switch has to be normally open, which means that the gate needs a weak pull-down resistor. Also, a gate series resistor is needed to limit the inrush current. Since the GPIOs of the ESP32 are capable of delivering 40 mA, any resistor value above 82.5 Ω limits the current enough. 470 Ω are chosen for the series resistor and 22 kΩ as the pull-down resistor.

SW2 is a high-side switch and it must be implemented with a P-channel MOSFET (FET1). The switch has to be normally open, which means that the gate must be pulled up to the source voltage, which is the voltage of the PV panel. The GPIOs of the ESP32 are not able to produce a high enough voltage to drive FET1 in these conditions, so an N-channel MOSFET (FET2) is needed. The proposed configuration can be seen in Figure 8.

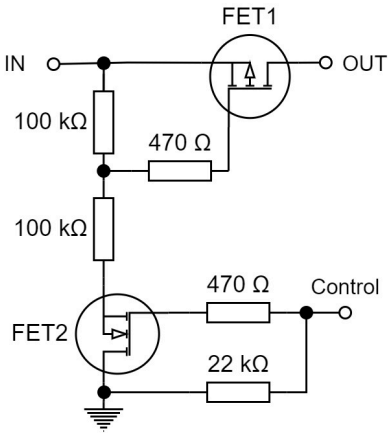

Figure 8: Electronic implementation of SW2 from Figure 2

FET2 is controlled in the same way as SW1. When the FET2 is blocking, the V_{GS} of FET1 is 0 V. When FET2 is conducting, the V_{GS} of FET1 is half the source voltage, half the PV panel's voltage. The PV voltage must be halved to limit V_{GS} below the absolute maximum rating for the DMP3130LQ-7 model.

The modifications to the ESP32-Devkit-LiPo board imply regulating the battery charging current, adding a charge status sensing capability, and isolating the USB connector's power path.

To regulate the battery charging current, R4 from Figure 3 has to be removed and substituted by a variable resistance circuit since the charging current depends on the resistance connected to the PROG pin of the BL4054B-42TPRN according to the formula $I_{CHRG}[mA] = 1000/R_{PROG}[k\Omega]$ (Shanghai Belling, 2009). A sophisticated solution would be to connect a digital potentiometer. However, a simpler solution is preferred because there is no need for optimal solar power harvesting. The proposed circuit is shown in Figure 9.

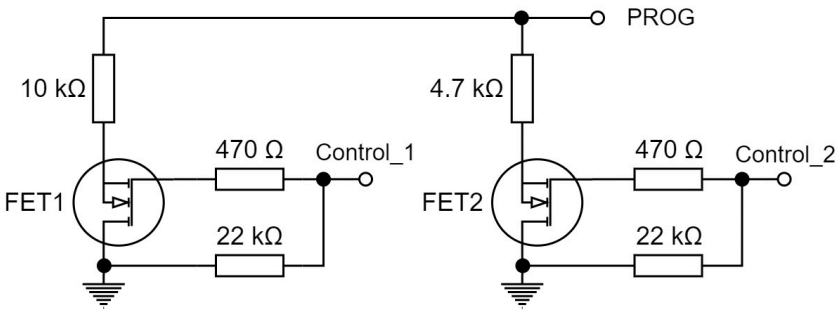

Figure 9: Triple-value resistance to control the charging current of a BL4054B-42TPRN

The circuit needs two digital inputs to control the charging current. FET1 can connect or disconnect a 10 kΩ resistor and FET2, a 4.7 kΩ. The behaviour of the system is summarised in Table 3.

Table 3: Behaviour of a BL4054B-42TPRN with the circuit from Figure 9 connected to the PROG pin

Control_2	Control_1	R_{PROG}	Charging
LOW	LOW	Floating	Stopped*
LOW	HIGH	10 kΩ	at 100 mA
HIGH	LOW	4.7 kΩ	at 213 mA
HIGH	HIGH	3.20 kΩ	at 313 mA

*When the PROG pin is left floating, the charging is stopped.

Low current values were the target for two main reasons: slower charges tend to prolong battery life (Kim et al., 2018), and charging can be guaranteed even in low irradiance conditions. Also, the ability to stop charging at will is a valuable feature.

The BL4054B-42TPRN includes a charging status pin (CHRGb) which is used with a LED indicator on the ESP32-Devkit-LiPo board. A connection was made from the CHRGb pin to the GPI34 pin of the ESP32 SoC to add a charge status sensing capability for the ESP32. The connection was made by soldering a thin cable between two vias on the PCB, as shown in Figure 10.

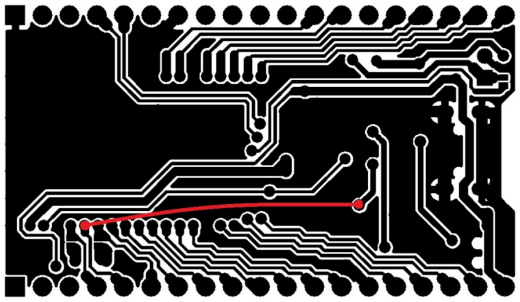

Figure 10: Wire (red) added to the bottom side of the ESP32-Devkit-LiPo Rev. C board

The only factor to consider is that the cable needs to be isolated and thin enough to fit inside the vias. This process is reversible since the cable can be removed at any moment.

Finally, isolating the USB connector's power path is necessary to be able to debug the device without charging the battery. The isolation can be done by removing D1 from Figure 3. This prevents the USB connector from supplying power to anything but the CH340T chip.

The pyranometer is designed as a separate module, considering it is only an optional element for the solar logger. Therefore, the absence or presence of the pyranometer and its peripherals must not affect the behaviour of the rest of the electronics.

Since the pyranometer uses a thermocouple, it does not require external power to react to environmental changes. The power supply is only needed for the internal electronics, which convert the thermocouple voltage with a 24-bit ADC, compute the irradiance, store the value, and enable Modbus communication. Given the case, powering the pyranometer module only 0.4 seconds before wanting to measure is enough because the device is programmed to make conversions at 10 Hz and store the average of the last four conversions (Hukseflux Thermal Sensors, 2021).

Having P-channel MOSFET as a high-side switch for the whole module's power supply makes this module more energy efficient. In this case, there is no need for an N-channel MOSFET to drive the P-channel MOSFET's gate because the maximum source voltage expected is 3.3 V, which can be matched by a GPIO of the ESP32 to block the MOSFET.

An important consideration is that the inrush current of the MAX8569AEUT+T and the capacitors might generate a brownout to the ESP32. A soft start can be implemented by selecting a huge gate series resistor for the MOSFET. The DMP3130LQ-7 model has a gate charge of about 6 nC (typical value). With 1 MΩ, the switching time should be about 2 ms, which is, empirically tested, enough time to avoid a brownout.

The final schematics are done in Autodesk EAGLE because then the PCB can be done based on the schematic. The complete schematic for the system can be found in Appendix 2, except for the pyranometer module, which can be found in Appendix 4. The list of materials for the respective PCBs can be found in Appendix 3 and Appendix 5.

4.4 Implementation: PCB design

With the schematics done, the PCB can be designed to implement the final state of the hardware. Two PCBs are created: one for the main device and one for the pyranometer's module. The PCBs are manufactured manually with chemical etching using pre-sensitized (positive photoresist) boards with 35 µm of copper. The designs are limited to a single layer for ease of manufacturing. No soldermask or silkscreen is done due to a lack of equipment and material.

The PCB design of the pyranometer's module can be seen in Figure 11, and the one for the main circuit in Figure 12. The drill holes are not included for simplicity. The legend for both figures can be found in Table 4.

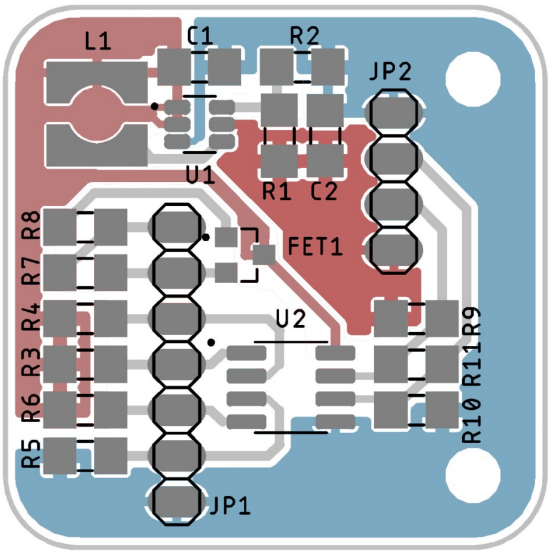

Figure 11: PCB layout of the pyranometer module with the copper layer, soldermask, and silkscreen

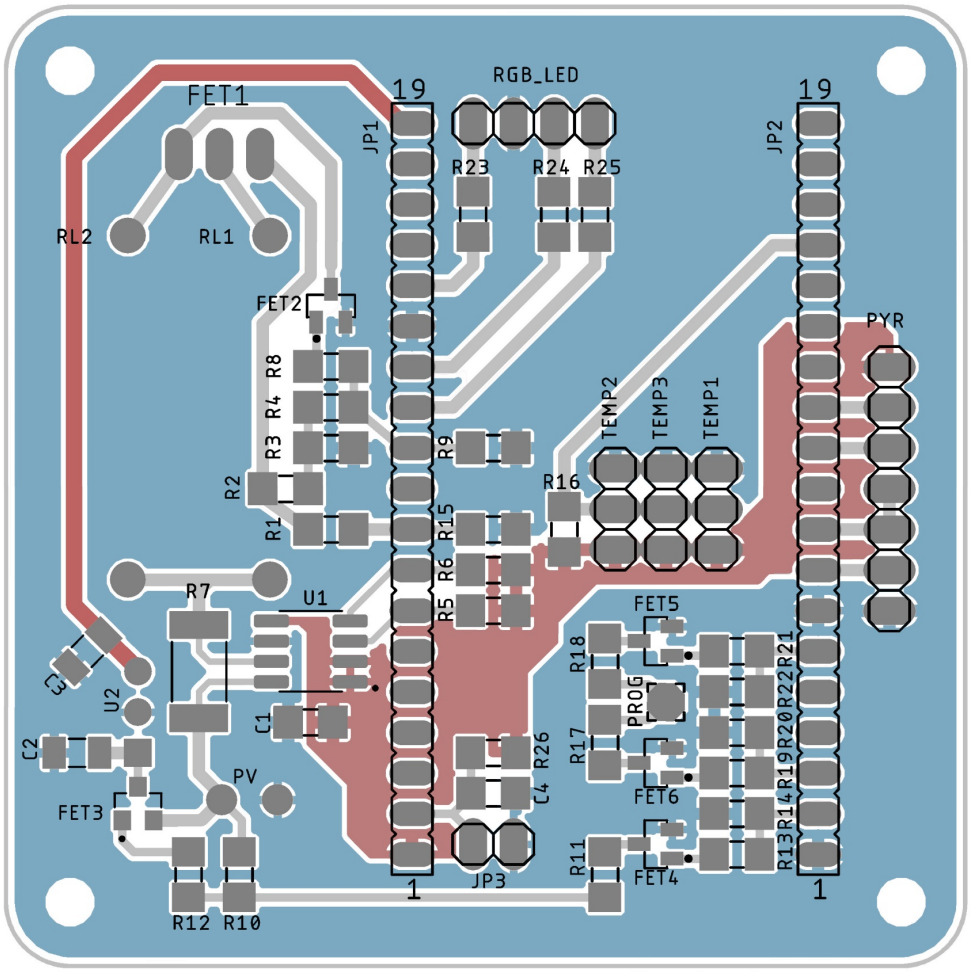

Figure 12: PCB layout of the main circuit with the copper layer, soldermask, and silkscreen

Table 4: Legend for Figure 11 and Figure 12

Colour	Meaning	Colour	Meaning
	Ground copper plate/traces		Signal traces
	3.3 V copper plate/traces		Soldermask
	5 V copper plate/traces		Silkscreen

The PCB of the pyranometer module is a 30x30 mm board with rounded edges (4 mm radius). Two 2 mm mounting holes have been added at the rounding centre of the corners. For the layout, the following aspects have been considered during the design:

1. All the passive components for the MAX8569AEUT+T (U1) have been placed as close as possible to the chip, minimizing the trace length.
2. The MAX3483AEASA+ (U2) has been placed in different board areas to avoid interferences from the inductor and capacitors.
3. The power supply is done with copper plates instead of traces whenever possible to reduce power losses or voltage drops due to daisy-chaining (Dokter, 2013).
4. The signal traces are done with a trace width of 20 mil (one thousand of an inch) whenever possible and reduced to 15 mil when necessary. 15 mil wide traces are more than wide enough for the expected currents since these traces can carry about 1.25 A with a 10˚C temperature increase (Jones, 2004).

5. Clearance is kept at 12 mil providing enough isolation for voltages above 30 V, way above the voltages the circuit handles.

The main PCB is a 60x60 mm board with rounded edges (4 mm radius). Four 2 mm mounting holes have been added at the rounding centre of the corners. For the layout, the following aspects have been considered:

1. The power supply is done with copper plates instead of traces for the same reason mentioned before. However, the 5 V supply is done with a single 40 mil trace, which can carry about 2.5 A with a 10˚C temperature increase (Jones, 2004).
2. Every signal trace is kept as short as possible. Some especially sensitive connections have been prioritized. These are the analog signal of the DAC and the shunt resistor's Kelvin contacts (Leibson, 2018).
3. The short signal traces are done with a trace width of 20 mil, reduced to 15 mil when necessary. Longer traces and the connections to the PV panel and the load are made with 30 mil traces when possible.
4. Since this board combines SMT and THT, the space was carefully utilized. For example, the temperature sensors have their connectors under the ESP32 board, which will be connected with two 1x19 pin sockets.
5. Clearance is again kept at 12 mil.

The finished boards can be seen in Figure 14 and Figure 13.

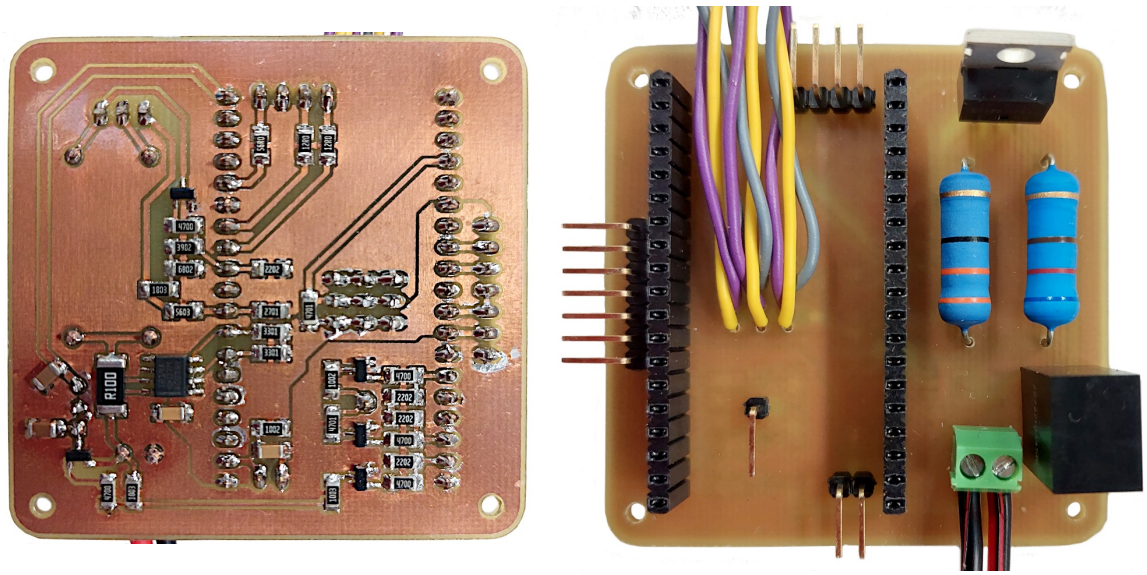

Figure 13: Main PCB of the solar logger populated

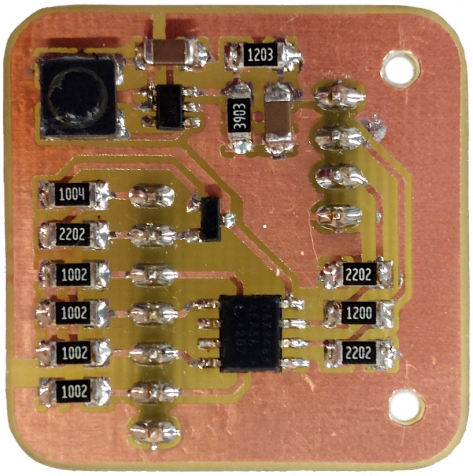

Figure 14: Pyranometer module's PCB populated

All the components were easily soldered by hand. Even though there was no soldermask, the solder was mostly kept on the pads thanks to the neck-downs for wide traces and thermals for pads connected to copper pour areas. On the Main PCB, the temperature sensors were soldered (through cables) to the board because including connector pins would have resulted in space problems.

The hardware design files, including the schematic, PCB layout, and libraries for Autodesk EAGLE, can be found in the following Novia-specific Microsoft OneDrive repository (click here) under the *Project PCB designs* folder.

5 Software design and implementation

In this section, the programming environment used is justified, and the final program's structure and working principle are discussed.

5.1 Programming environment

The selection of the programming language, code editor, and integrated development environment (IDE) used for a project is important and should be considered carefully.

The official programming languages used for the programming of Espressif boards are C or C++ because the official compiler is meant for these languages. Third-party interpreters for various other languages like Python or Lua are also available (smartswitchsio, 2018). The author is most familiar with the C language and thus is the chosen working language.

Two of the available frameworks are the Arduino Framework and the ESP IoT Development Framework (ESP-IDF). Arduino Framework has the advantage of having a larger community and more libraries available. On the other hand, ESP-IDF is native to Espressif boards and is well-documented by the company. The latter is chosen because of the nativity and the future development possibilities.

A common IDE option to program Espressif boards is the Arduino IDE. But using the PlatformIO IDE extension for Visual Studio Code is more suitable for large and multifile programs and has more functionality (DroneBot Workshop, 2021). Thus, PlatformIO is used for this project.

5.2 Program working principle

This section aims to explain how the program works and how every functionality is achieved. For clarity, the program is split into setup, measurement, transmission, connectivity tasks, and power management parts.

The program takes advantage of the built-in real-time operating system (RTOS) of ESP-IDF. The RTOS is a modified version of FreeRTOS that can run on both cores of the ESP32. Using an RTOS, the program flow can be manipulated at will using tasks and inter-task synchronization and messaging tools, such as event groups or queues. The main advantage of using an RTOS is that apparent parallelism between tasks can be achieved with fast switching between tasks. FreeRTOS is a complex software and will not be described in this work.

5.2.1 Setup

The setup code runs only at the beginning of the first boot. It performs calibration and test routines to ensure that the system is prepared to function correctly. Then the ESP32 enters deep sleep until the time of the first measurement. The specific routines that are performed are:

- Connectivity tests. The ESP32 tries to connect to Wi-Fi, then to the MQTT broker and tries to publish a message, then to the SNTP server to synchronize the system time, and then makes an HTTP request for sunrise and sunset data. Each of the connectivity tasks is described in Section 5.2.2. The test succeeds if all the actions can be performed, not necessarily on the first try.

- ADC calibration for battery voltage measurement. The ESP32 checks if ADC calibration values are burnt into the eFuse, and then performs the ADC-voltage curve characterisation. The characterisation data is stored in the RTC slow memory to avoid running the calibration process every time a deep sleep reset occurs.

- Test of the INA219 sensor. The ESP32 tries communicating with the INA219 chip and sets it to shutdown mode. The test succeeds if the communication is successful.

- Test of the DS18B20 sensors. The ESP32 scans for DS18B20 devices and checks whether the found devices' addresses match the expected ones. The devices' addresses must be known because the three sensors perform different measurements and are connected to the same 1-wire bus.

- Test of the pyranometer. The ESP32 powers the pyranometer module and attempts communication by requesting its slave address. The test succeeds if the communication is successful and the returned address matches the address used for the communication. If the test succeeds, a bit is stored into the RTC slow memory, so the program will know that a pyranometer is connected. Elsewise, the program proceeds as if no pyranometer were to be connected.

If all tests succeed, the setup is considered successful. The first measurement is synchronized to be a multiple of the measurement period according to Unix time, and the ESP32 enters deep sleep until then. Elsewise, the boot count is reset, and the setup is repeated after one minute of deep sleep.

5.2.2 Connectivity tasks

There are four connectivity tasks performed in the program. The connectivity tasks are run in parallel to improve time efficiency, and synchronization between tasks is achieved with FreeRTOS events. The flow diagrams of the connectivity tasks, with the FreeRTOS events in grey, can be seen in Figure 15.

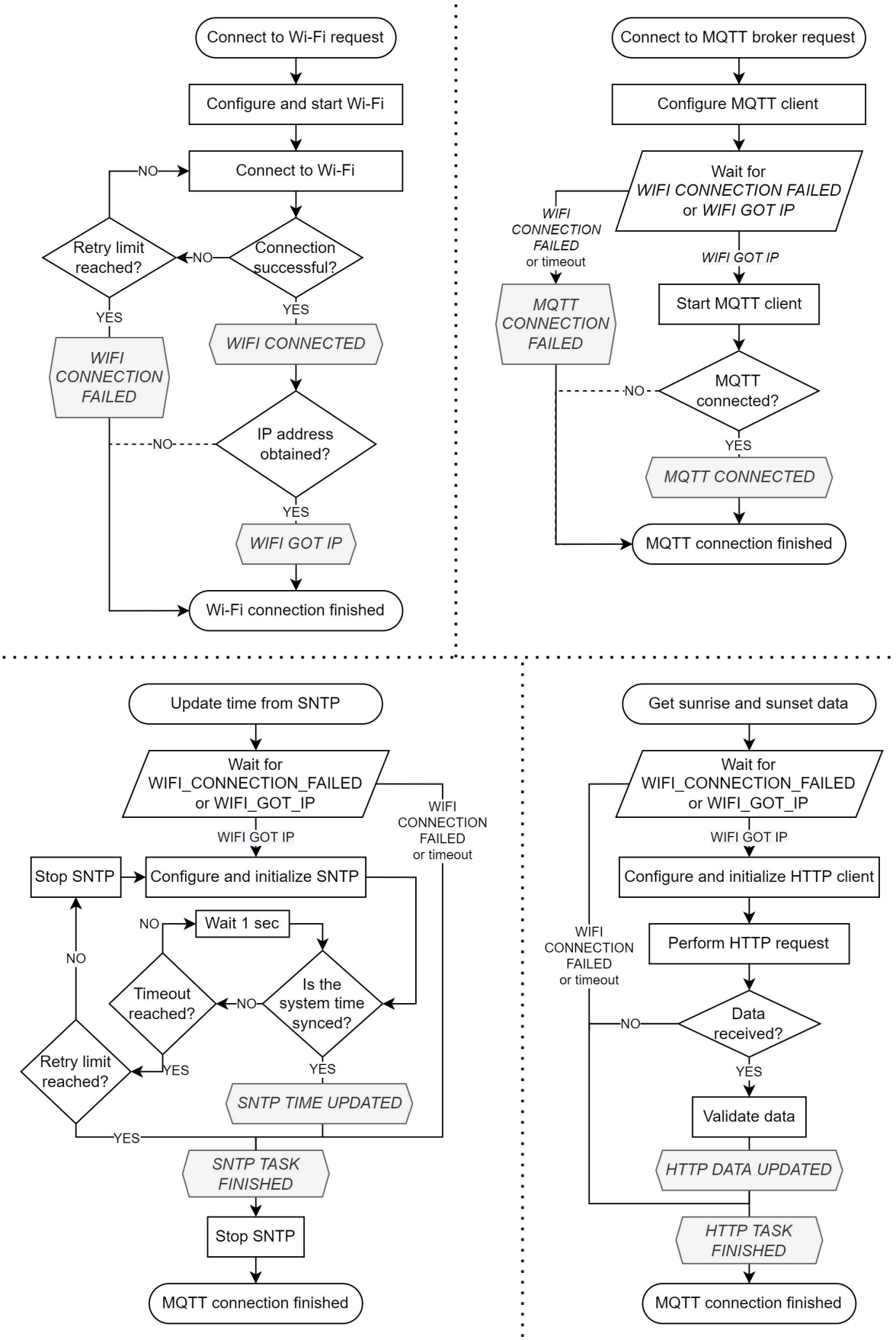

Figure 15: Flow diagram of the connectivity tasks

The first task is connecting to Wi-Fi: a requirement for the other three. Connection attempts might fail. Therefore, a retry system is implemented, which retries the connection up to five times before aborting the operation. Another function handles the disconnection.

The second task is to connect to the MQTT broker. Novia UAS uses a Mosquitto broker with host iot.novia.fi. This connection process is aborted if the Wi-Fi connection fails or times out. The publishing of messages and the disconnection of the client is handled separately.

The third task is to update the system time from an SNTP server. The server used was pool.ntp.org. Again, this process is aborted if the Wi-Fi connection fails or times out. The system time is updated automatically upon connecting to the SNTP server, but sometimes the response is delayed or denied. The sync status is pulled every second to know when the system time is updated (no event-based structure could be implemented). If the process times out, reconnection to the server is attempted to generate a new request.

The last task is the HTTP request for sunrise and sunset data. The API used was https://sunrise-sunset.org/api, which returns a JSON object containing the sunrise and sunset times in UTC+0, among other information). Again, this process is aborted if the Wi-Fi connection fails or times out. Three HTTP requests are made: for the current day and the two following days. Then, the data is contrasted to obtain useful data. The contrast is necessary to correct for time zone and high latitude occurrences[3]. The sunrise and sunset time data is stored in the RTC slow memory.

By having parallel tasks, the slowest process dictates the total execution time of the connectivity processes. The slowest process is the system time updating because the SNTP server's response can be delayed.

5.2.3 Measurement

Several parameters are measured: system time, battery voltage, various temperatures, PV characteristics, and irradiance (if a pyranometer is connected). The measurements are done in series to prevent information losses while transmitting or receiving information over the different digital channels.

The system time is measured in Unix time as a 32-bit signed integer, the way time_t is defined in the *time.h* library. That means that overflow problems will appear in 2038. Adapting the time format to 64-bit signed would solve this problem.

The battery voltage is measured with ADC1. The ADC-voltage characteristics stored in the RTC slow memory are used to convert the raw ADC conversions to mV. 64 consecutive measurements are taken and averaged. Since the battery voltage is measured through a

[3] Sunset time for certain days can occur the following day if UTC+0 time is used.

voltage divider that divides by 2, the ADC measurement needs to be multiplied by 2 to get the real voltage. The voltage value is stored in mV as a 16-bit unsigned integer.

The temperature sensors are read using the ds18x20.h library from the esp-idf-lib. The DS18B20 sensors require about 750 ms to perform a conversion once a measurement is requested. The temperature values are stored as float values in ˚C.

The load is connected to characterise the PV panel. The INA219 is configured to work in triggered measurement mode for shunt and bus voltage, with 12-bit conversions and an averaging rate of 32 samples. The shunt and bus voltage measurements each take 17.02 ms in this mode. The DAC output, which controls the load's value, is ramped up from 0 to 252 with steps of 4 units (64 values) with 75 ms between each step. When an INA219 conversion is triggered, a delay of 40 ms is introduced to wait for the conversions to finish (it should last two times 17.02 ms). Then the DAC value is increased again. This timing leaves 35 ms for the PV voltage and current to stabilize. The whole characterisation takes less than 5 seconds. Both the shunt and bus voltages are stored as arrays of raw values to save space. The shunt voltage is stored as a 16-bit signed integer, each unit indicating 10 µV and the sign representing the sense of the current. The bus voltage is stored as a 16-bit unsigned integer, each unit indicating 4 mV.

The irradiance is only measured if the pyranometer module is connected. The irradiance value is retrieved from the pyranometer and stored as a 32-bit signed integer, each unit indicating 10 mW/m^2. Negative values mean that the pyranometer is irradiating instead of absorbing heat.

The order of the measurements is meditated. The pyranometer module is powered on at the beginning (if appropriate). The time is fetched first, so the time indicates when the measurement began. Then the battery voltage and temperatures are measured before retrieving the irradiance to leave time for the pyranometer to perform some conversions (if appropriate). At this point, the pyranometer module is shut down (if appropriate). Finally, the PV characterisation is performed.

All the data for one measurement sequence is stored as a structure within which each field is one of the measured magnitudes in the beforementioned formats. An array of these structures is stored in the RTC slow memory and is overwritten after a data pack is published to the MQTT broker. The RTC slow memory has 4 kB of storage available. 278 bytes of storage are required to store one structure, meaning an array of 14 structures can be stored before the data needs to be published to the MQTT broker. The maximum number of structures to be stored before publication can be defined.

5.2.4 Transmission

The transmission is done when the maximum number of data structures stored is reached or when the last measurement before going to deep sleep overnight is done. The ESP32

performs all the connectivity tasks (except the HTTP request for sunrise and sunset data, which is done only once a day) since a Wi-Fi connection is required anyway. All the data structures are serialized as JSON to ease the processing at the receiving end. Once the MQTT client is connected to the broker, the JSON string is published. The JSON string contains the following for each of the data structures:

- The time when the measurement was initiated in ISO 8601 as a 20-character string.
- The battery voltage in mV as an unsigned integer.
- If a pyranometer is connected, the pyranometer value as a signed integer, each unit indicating 0.01 W/m^2.
- The PV panel temperature as a floating-point value with two decimal places in ˚C.
- The battery temperature as a floating-point value with two decimal places in ˚C.
- The air temperature as a floating-point value with two decimal places in ˚C.
- The shunt voltage measurements as a 64-position array where each value is a signed integer, each unit indicating 10 µV.
- The bus voltage measurements as a 64-position array where each value is a signed integer, each unit indicating 4 mV.

5.2.5 Power management

The system can be in three different power states:

- BATTERY. Running on battery power because the battery voltage is higher than 3.3 V (programmable threshold). This state continues until the battery voltage falls below the threshold.

- CHARGING_NEEDED. Running on battery power but in need of charging because the battery voltage is lower than 3.3 V or was in the process of charging, but there is not enough solar power available. This state continues until solar power is available, and the charging can start/continue.

- CHARGING. Running on PV power and charging the battery because its voltage reached the 3.3 V charge limit and there is enough solar power. This state continues until the battery is fully charged, even if it can be interrupted by the lack of solar power.

It might be counterintuitive to use battery power always except when the battery needs charging but using PV power whenever available would hold the battery with a constant charge over long periods, which can result in a fast decrease of capacity for high charge states (Battery University, 2021). Constant cycling is a better approach in this case.

When the charging of the battery begins, the adequate charging current is selected first by trying in descending order how much current the PV panel can deliver still keeping its

voltage above 6.5 V. When the voltage drops below 6.5 V, the charging must be interrupted (leaving the PROG pin floating) to allow the PV panel to recover its voltage.

Once the charging current is selected, a charging monitor FreeRTOS task is created, which uses the INA219 to scan at 2 Hz the PV panels voltage. When the voltage falls below 6.5 V, the charging is reset, and the program tries to find an adequate charging current. Suppose no charging current can be maintained with more than 6.5 V (meaning there is insufficient PV power). In that case, the program retries the process in 2 seconds to ensure it is not only a temporary absence of solar irradiation (a bird flying over the panel, for example).

The power state management is controlled by a FreeRTOS task that runs on Core 1 and implements a FreeRTOS queue handler. The handler waits for elements to be added to the queue and performs the corresponding action. The elements of the queue act like commands and can have appended data. There are five commands:

- MEAS_STARTED. This command is sent right before a measurement routine is performed. If the power state is CHARGING, the handler temporarily stops battery charging, so the PV power is available for the I-V characterisation.

- MEAS_FINISHED. This command is sent right after a measurement routine has finished. If the power state is CHARGING, the handler resumes battery charging since the PV power is no longer required for the I-V characterisation. If the power state is BATTERY, the handler checks the last reported battery voltage and changes the power state to CHARGING if the voltage is below 3.3 V. If the power state is CHARGING_NEEDED, the handler checks if the last reported maximum PV power is higher than 750 mW, meaning it would be enough power to resume charging.

- CHARGING_FINISHED_QUERY. This command is sent if the CHRGb pin of the BL4054B-42TPRN is high, meaning that the chip has stopped charging. The handler waits 100 ms and double-checks the state of the CHRGb pin to ensure it is not a false signal, which can occur due to oscillations of the PV power.

- NO_SUN_AVAILABLE. This command is sent if the solar power falls below the minimum amount to charge the battery at 100 mA while still holding a voltage above 6.5 V (minimum input voltage for the V7805-1500 converter). The handler stops the charing and changes the power state to CHARGING_NEEDED.

- DEEP_SLEEP_REQ. This command is sent after the next measurement time is determined. The handler starts deep sleep until the next measurement needs to be done if the power state is not CHARGING to preserve the battery. The timing information is passed on as data alongside the command.

The logger is expected to be in deep sleep most of the day and all night. An algorithm calculates when the device needs to be woken up next. After each measurement, the algorithm checks if the sun has set and decides if the next wakeup time will be in the next

measurement period or at sunrise. The algorithm also has to compensate for time jumps caused by the system time update[4] and determine when the sunrise and sunset data need updating.

5.3 Program structure

The full project code is split into different files and organized in folders. The default structure when creating a project with PlatformIO includes the *lib* folder for project-specific libraries, the *include* folder for header files, and the *src* folder for all the source files for the project. Figure 16 represents the folder structure for the header and source files and the dependency diagram of the header files and the main source file.

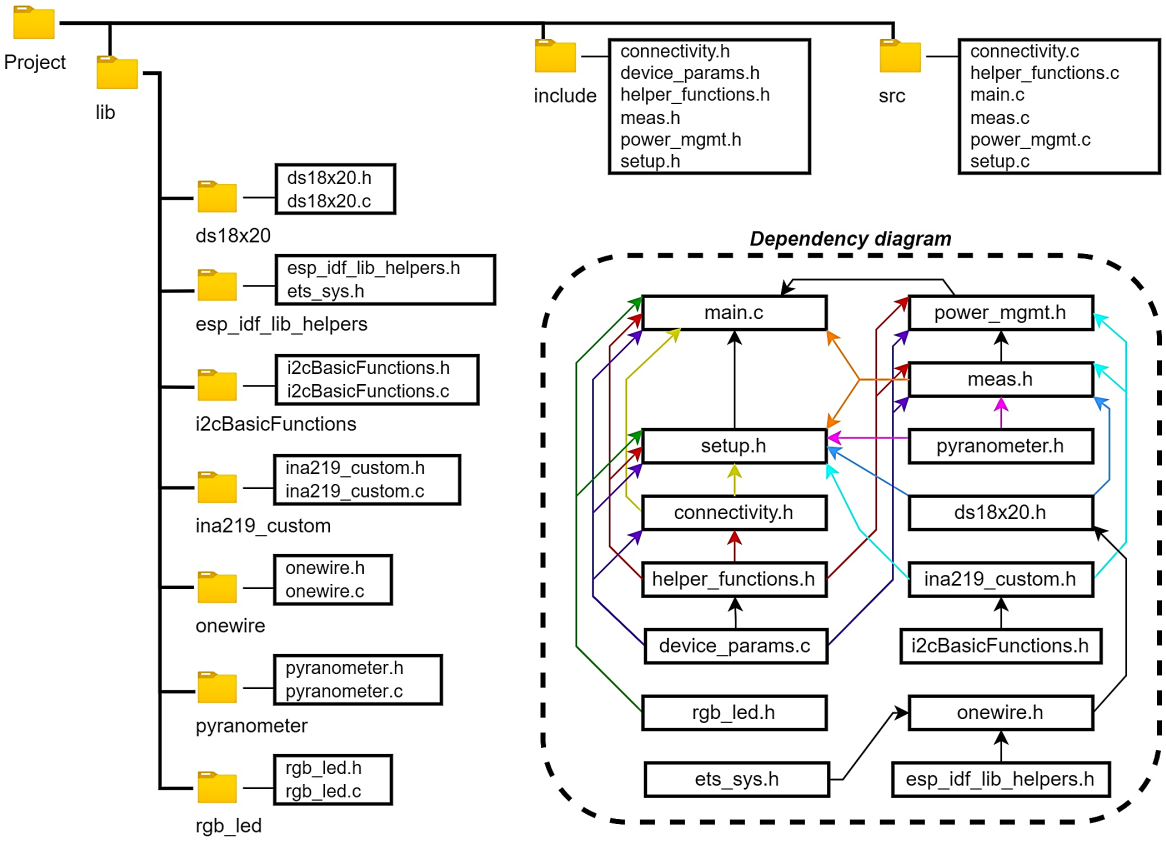

Figure 16: Project hierarchy (only header and source files) with file dependence diagram

From the *lib* folder, all libraries are custom-made except the *ds18x20* library (including its dependencies). The custom-made libraries can be reused in other projects; thus, they are libraries. The files from *include* and *src* are pieces of the data logger's algorithm and are prepared to work together. Splitting the whole code into pieces makes the code modular and easier to debug and modify. The content of the files is the following:

[4] It has been tested that the ESP32, without an external oscillator, can have a delay of about 20 s/h in the system time.

- *main.c* is the principal code. Most of the initializations and the setup, measurement, and connectivity routines are called in this file. The file dictates the general flow of the algorithm.

- *meas.c* (and *meas.*h) contains all the code to perform the specific measurement processes. It includes functions to get the system time, perform the PV characterisation, get the temperature values, get the battery voltage, compute the maximum power generated, and JSON-serialize the measurement structure array.

- *connectivity.c* (and *connectivity.h*) contains all the code to perform the connectivity tasks from Section 5.2.2. This file includes caller functions to start each task; the routines themselves; event handlers for Wi-Fi, MQTT, and HTTP events; an MQTT publishing function; and a JSON deserializer for the sunrise and sunset data.

- *power_mgmt.c* (and *power_mgmt.h*) contains all the code to perform what was described in Section 5.2.5 (except for the sleep intervals, handled in *main.c*). The file includes the queue handler, the charging monitor task, and functions to select the charging current and to start/stop the charging.

- *setup.c* (and *setup.h*) contains the functions that perform the routines listed in Section 5.2.1. The file also includes functions to synchronize the first measurement and handle any errors during setup.

- *helper_functions.c* (and *helper_functions.h*) contains error handling macros and small functions for tasks performed frequently in other functions, like powering on the pyranometer.

- *device_params.h* contains definitions of general parameters of the system like the GPIO numbers used for each functionality, Wi-Fi and MQTT credentials, the GPS coordinates, and general configuration values (measurement period and memory queue, device addresses…). It is especially comfortable to have all these parameters in one file.

All the project files, except the builds, can be found in the following Novia-specific Microsoft OneDrive repository (click here) under the *Project code* folder.

6 Case design

A case is needed to isolate the electronics from the exterior and unify all components of the logger into one device. The concept is simplistic: a box with mounting brackets for both the solar panel and ground, several waterproof holes, and mounting structures for the PCBs.

An overview of the proposed design can be seen in Figure 17. The structure on the left is the cover and will be attached to the solar panel. The structure on the right is the base and will be attached to the ground.

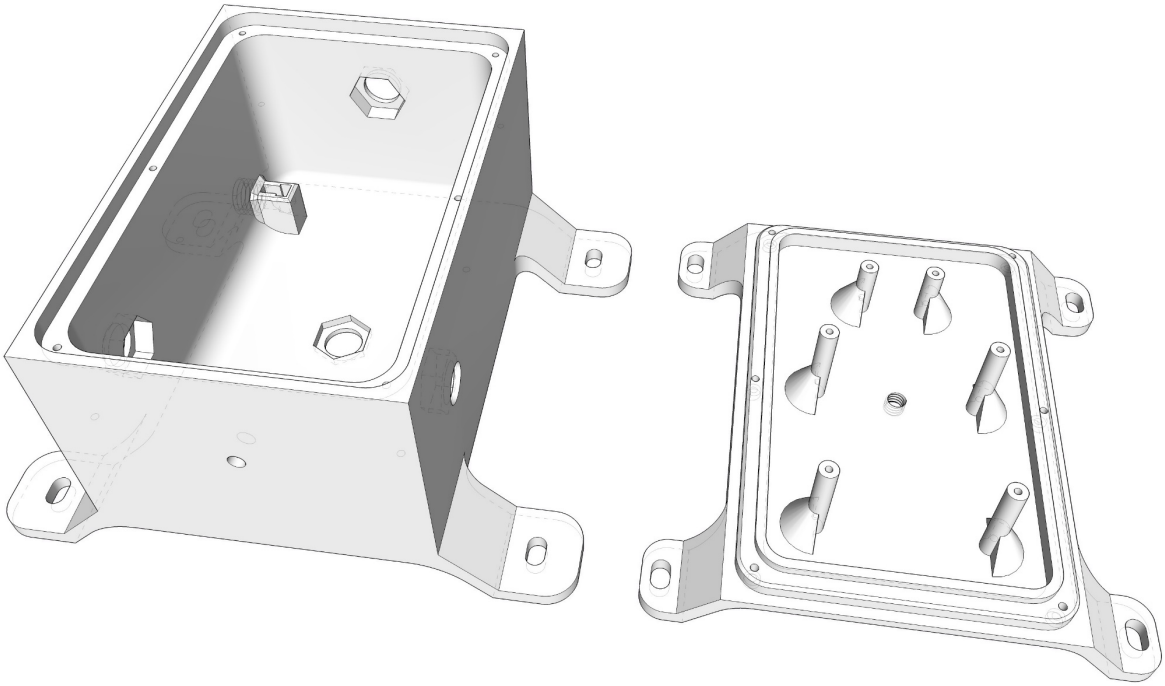

Figure 17: Overview of the two main parts (cover on the left, base on the right) of the case for the logger

The base and the cover will be pressed together with six M2 bolts. There is a gap between the two parts (generated by a 1 mm chamfer on the base) enough to fit sealing rubber 1 mm in diameter. The rubber will be tightened in the corner of the step in the cover, sealing the joint. The fit between the two parts has two right-angle steps in a way that makes water leakage difficult. The features of each part are summarised in Table 5.

Table 5: Features of the base and cover of the case

Features of the base	Features of the cover
• Four mounting brackets are prepared for M6 bolts (first mounting option). • A camera mount screw hole (through hole with 1/4" – 20 UNC thread) in the middle of the base (second mounting option).	• Four mounting brackets for the PV panel (with M6 bolts and nuts). • One 5 mm through hole for the indicator LED (press fit). • Four 12 mm through holes with 3 mm deep hexagon shape blind holes, prepared for M12x1.5 cable glands.

Features of the base	Features of the cover
• Four 30 mm high mounting structures for the main PCB with 25 mm deep 1.9 mm blind holes for M2 bolts. • Two 20 mm high mounting structures for the pyranometer module with 15 mm deep 1.9 mm blind holes for M2 bolts. • Six 2 mm through holes with (at least) 2 mm deep 5 mm blind holes for M2 bolts to go through and hide the bolt heads.	• Six 30 mm deep 1.9 mm blind holes for M2 bolts. • A press fit holding structure for any 6x6x4 mm tactile switch with an actuator length up to 6 mm, with a 1/2" – 13 UNC threatened hole in front of the actuator so it can be accessed from the outside.

Most of the features require very high tolerance control during 3D printing. 3D printers rarely print small pieces of the same size as the model. To correct these differences, most features have been printed out isolated and replicated with minor size variations to experimentally determine which model size corresponds to the ideal size after printing. Of course, these corrections are printer-dependent.

Some auxiliary parts, which can be seen in Figure 18, were also necessary.

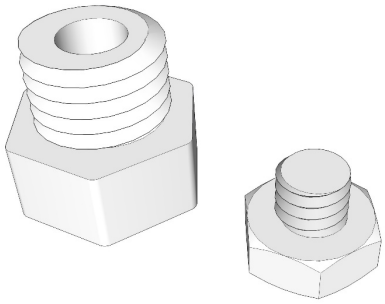

Figure 18: Auxiliary parts for the case

The piece on the left side is a 1/2" – 13 UNC bolt with 8 mm of thread to cover the hole for the tactile switch in the cover. The piece on the right is a 1/4" – 20 UNC bolt with 5 mm of thread to cover the hole for the camera screw on the base.

The 3D models with .skp extension for SketchUp and the .stl files for all the pieces can be found in the following Novia-specific Microsoft OneDrive repository (click here) under the *Case 3D models* folder.

7 Results

Due to time limitations, it was impossible to completely assemble the data logger because the final version of the case could not be printed. However, the electronic and software parts were finished and tested.

The data logger was tested indoors with incandescent lamps as a light source for the PV panel. Figure 19 shows the DAC voltage (CH1), PV voltage (CH3), PV current (CH4), and the PV power (product of CH3 and CH4) during the I-V characterisation process.

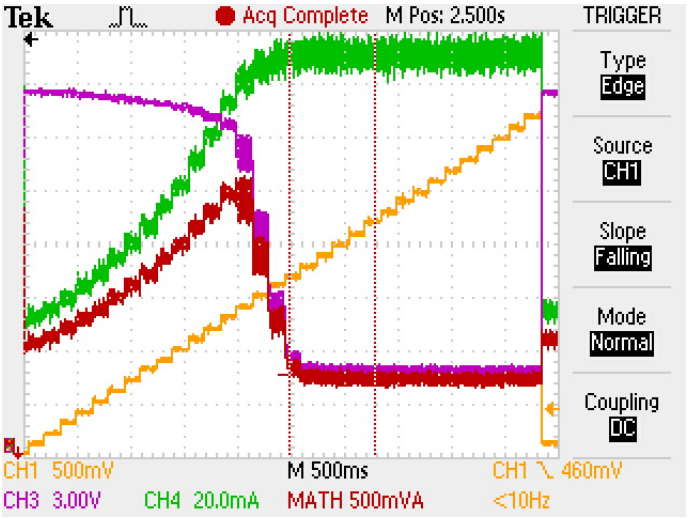

Figure 19: Signals during the I-V characterisation of the PV panel

The test was done with moderate[5] light, showing a clear power peak of about 2500 mW. The partiality of the I-V characterisation can be identified because neither the PV voltage nor the current reach zero, meaning the open-circuit and the short-circuit conditions are never reached. This partiality does not impede the identification of the MPP but increases the accuracy. Tests were conducted with other irradiance conditions, and even though the power peak was obtained for different DAC voltage values, the MPP was always identifiable for irradiances higher than 100 W/m^2.

The stability of the PV voltage and the accuracy of the INA219 chip were also tested. The test aimed to ensure that the PV voltage (and, at the same time, the current) was measured in a steady state and that the INA219 reflected the real value. Figure 20 and Figure 21 show the DAC voltage (CH1), the PV voltage (CH2), and an auxiliary signal that indicates the duration of the conversions for the INA219 (CH3).

[5] The exact irradiance was not measured but it was enough to generate about half the rated power of the PV panel.

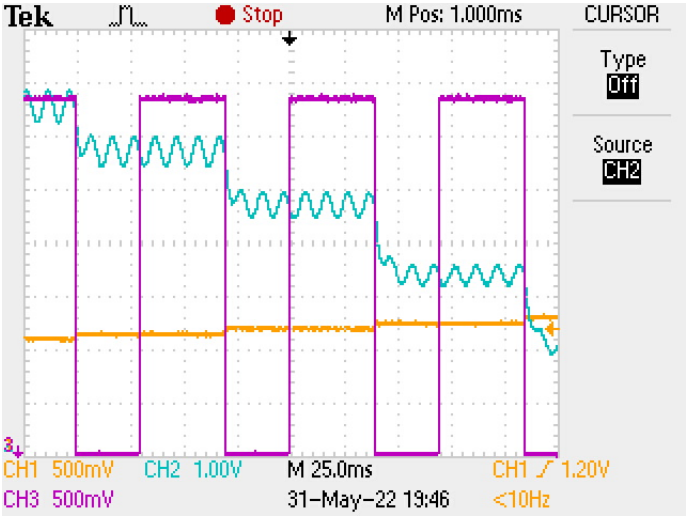

Figure 20: Signals during I-V characterisation when PV voltage has high values

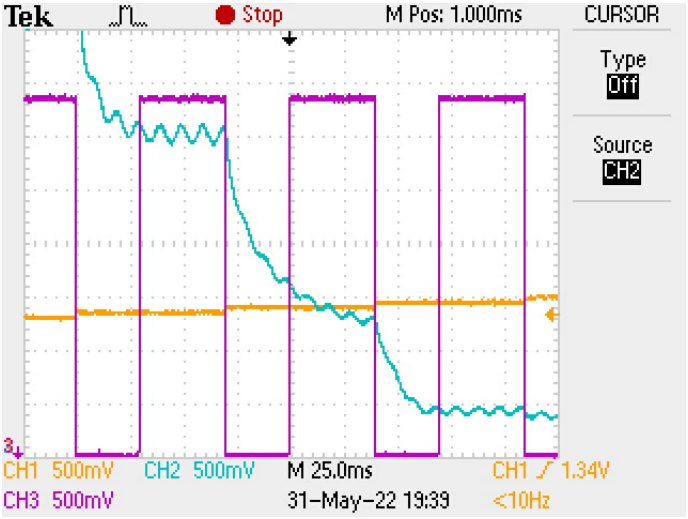

Figure 21: Signals during I-V characterisation when PV voltage has low values

The PV voltage has a sinusoidal oscillation due to the incandescent light's oscillation in intensity. Because the lamb used was connected to 230 V AV at 50 Hz, the lamp's light intensity oscillated at 100 Hz, which translated into oscillations of the same frequency in the PV voltage.

Figure 20 represents the early phase of the I-V characterisation when the PV voltage is still relatively high, while Figure 21 represents the phase when the PV voltage drops abruptly. Three conversions are fully captured in both cases. The voltage during the conversions is stabilized (ignoring the 100 Hz ripple) except for the second one in Figure 21. Because that measurement corresponds to a voltage value after the MPP, the uncertainty of the value will not critically influence the I-V characterisation. The numerical values of the PV voltage are contrasted in Table 6.

Table 6: Contrasting of the INA219 conversions with real values

Figure	Conversion	Oscilloscope average [mV]	INA219 conversion [mV]	Error (%)
Figure 20	1	9233	9168	0.70
	2	8227	8172	0.67
	3	6920	6884	0.52
Figure 21	1	3416	3408	0.23
	2	1729	1744	0.87
	3	825	848	2.79

The oscilloscope average is calculated over the period [17, 34] ms after the beginning of the conversions because the INA219 does the shunt and bus voltage conversion in series, beginning with the shunt voltage. Results show that the INA219 is reliable enough, with an error below 3% in all cases.

A long-term stability test showed that the ESP32 unexpectedly reset at some point after 200 boots (every time the device wakes up from deep sleep, it is considered a boot). This error can lead to data losses if it happens when there is data stored in the RTC memory which was not yet published. This phenomenon would require further investigation, even if it does not impede the logger from functioning.

To predict the device's autonomy without a recharge, the current consumption was measured in different phases of the program. Table 7 summarises the measured data.

Table 7: Current consumption characteristics of the solar logger

Phase	Current consumption avg.	Observations
Deep sleep	~80 µA	According to the respective manufacturers, the ESP32-Devkit-Lipo consumes 65 µA, from which the ESP32 SoC consumes 10 µA in deep sleep, and most of the deep sleep current is consumed by the SY8089AAAC regulator. The additional electronics consume the other 15 µA
Measurement	~70 mA (additional ~45 mA with pyranometer module)	The uncertainty of this measurement is high due to the lack of proper instrumentation.
Connected to Wi-Fi	~400 mA	The uncertainty of this measurement is high due to the lack of proper instrumentation. The results may vary depending on the connection strength.

The duration of the measurement phase is about 7 seconds. The duration of the connectivity tasks varies from time to time, but it is usually between 2.5 and 5 seconds, depending on the response time of the SNTP server. Longer times can rarely happen.

Considering a usual configuration and measurement scenario with a measurement period of 5 min., data packs of 12 measurement structures, daylight of 16 h, and night of 8 h, the expected energy consumption is summarised in Table 8.

Table 8: Consumption characteristics of the solar logger for one day with 16 h day length

Phase	Freq.	Duration	Total duration	Current consumption	Energy consumption
Deep sleep	N/A	N/A	84,976 – 85,016 s (23.604 – 23.616 h)	~80 µA	1.888 – 1.889 mAh
Measurement	5 min.	~7 s	1344 s (0.373 h)	~70 mA	26.11 mAh
Connected to Wi-Fi	1 h	2.5 – 5 s	40 – 80 s (0.011 – 0.022 h)	~400 mA	4.4 – 8.8 mAh
				TOTAL	**32.4 – 36.8 mAh**

With the 1400 mAh battery, the expected autonomy would be between 38 and 43 days, with the assumed configuration and day length conditions. With a measurement period of 10 min. instead of 5 min., maintaining the connectivity tasks period to 1 h, the consumption would be reduced by 13.06 mA, extending the autonomy by 29 – 31 days.

A battery management test was performed as well. This test showed that the adaptive-current charging functions as expected and can charge the device even in relatively low light conditions.

To manufacture this logger, the raw material (excluding PCB and case material) costs about 55 € and an additional 11 € for the pyranometer module (excluding the pyranometer). For a more exhaustive material list, see Appendix 6.

The PCB material and manufacturing would cost between 5 € and 10 € if it were to be done professionally by a Chinese PCB manufacturer like JLC PCB or PCBWay. The cost of the case highly depends on the material used and printer configuration (like filling density), which influences the volume of plastic used. Printed with PETg with infill of 20% and wall thicknesses of 0.5 mm, the base part weighs about 125 g and the cover 250 g. PETg costs about 30 €/kg, making the case cost around 10 €.

The whole device, without a pyranometer, can be manufactured for about 75 €. If the pyranometer module is included, the price increases by 11 € plus the price of the pyranometer used.

8 Discussion

Concerning the initial aim and objectives, they were mostly accomplished, lacking only the printing of the case and assembling. The specifications of the device have been met as follows:

- The device is based on an ESP32 board.
- The data is logged through the MQTT protocol to a broker.
- The data is collected and digitalised reliably. The validity of the data for the purposes is assumed but can only be proved after analysing data over an extended period of time.
- The device is relatively small. The case's main body (excluding mounting brackets) is a 159x105x85 mm box with a 245x193x18 mm solar panel on top of it.
- The case is prepared to be waterproof and resistant to UV light.
- Predictions showed about 40 days of autonomy without recharging with a 5 min. measurement period. This time increases to about 70 days with a 10 min. period. The recharging functionality should make the device's autonomy unlimited.
- The cost of the device, without a pyranometer, is about 75 €. The device is then cheaper than traditional logger devices with solar irradiation sensors.

Three of the four objectives were entirely accomplished. A study about the different solar irradiation sensors showed that using a solar panel as a sensor should provide enough information for solar panel installation feasibility studies while being low in price. A PCB has been successfully designed and manufactured for the system. A battery-optimised software (combined with adequate hardware) provides extended battery life.

The fourth was only partially accomplished. The manufacturing of the case could not be done. However, 3D models have been developed to enable 3D printing and assembly at a later date. It is estimated to cost around 10 € and takes about 24 h for the cover and 12 h for the base to be printed.

Possible improvements to the current design are:

- Including an external NVS (like and microSD card) would allow the device to work in areas without connectivity. However, other issues like the system time desynchronization also need to be solved to fully enable offline functioning.
- The hardware design could be done using an ESP32 chip instead of a development board, further integrating the electronics.
- Some components, like the 744042100, the MAX8569AEUT+T, and the V7805-1500, could be substituted for cheaper components. The switching transistors could be substituted for cheaper models appropriate for the current rating of their usage.
- The case could be further size optimised.

- The PV panel's I-V characterisation can be improved by implementing a ramp-up followed by a ramp-down characterisation with posterior averaging.
- An I-V characterisation fault detection algorithm can be implemented to detect irregularities in the measured data, like a sudden voltage drop caused by a bird flying over the panel and partially shadowing it.
- By using a faster ADC for bus and shunt voltage measurements, faster I-V characterisation can be achieved, consequently reducing energy consumption.

In contrast with other low-cost solar loggers present in the literature, the device proposed in this work differs from most because of the magnitude measured and the power management system.

The devices presented by Oliveira et al. (n.d.) and Rocha et al. (2021) require an external power supply, while the ones presented by Vera et al. (2005) and Effendi et al. (2018) use a battery but require an external recharge. The device presented in this work can potentially achieve complete autonomy unless low-temperature conditions (below zero degrees Celsius) impede recharging.

Harvesting solar energy to power sensor devices is an actively used and optimised concept, although it is more common in wireless sensor nodes. Powering devices only with solar panels can be done with or without energy storage (He et al., 2009; Zhang et al., 2016). The energy management system of the presented device is not as sophisticated and optimised as some examples in the literature, but it is sufficient to maintain the device running wireless for, supposedly, unlimited time.

As for the measured magnitude, logging I-V characteristics of a solar panel is, compared to the literature, a less common practice than extracting an approximated irradiance value from any sensor's measurable parameters. Cruz-Colon et al. (2012) and Chen et al. (2012) state that the irradiance value can be approximated by characterising a PV panel.

The approach chosen in this work is to log raw I-V characteristics of the PV panel, enabling any post-processing. Simple modifications to the PCB, like removing RL2 and shorting RL1, can enable near short-circuit current and open-circuit voltage measurements if necessary. The advantage of this approach is that the data manipulation duty is transferred to the receiving end of the data at the cost of increased storage space since storing the entire I-V characteristics requires more memory than storing, for example, the maximum power.

Regarding cost, the only references are the devices presented by Oliveira et al. (n.d.) and Rocha et al. (2021). Compared to the former, the presented device is in the same price range (75 € compared to 50 $}. Compared to the latter, the presented device is in a lower price range (75 € compared to 200 $} at the cost of reduced quality of measurements.

The most significant limitation of this work is that the validity of the data that is going to be collected can only be assessed after long-term usage of the device. Therefore, the

device's practicality is still unproven but is expected to be suitable for the given purpose. The device is supposed to provide power production statistics which then can be extrapolated to a system with a larger area or contrasted with data from another logger to do relative analysis.

Another limitation is that the software is only in the prototype phase, so it lacks a configuration interface: all configurations and credentials are hard coded in the program. Consequently, the code must be modified, compiled, built, and uploaded to the ESP32 to modify any parameter.

Moreover, the device is prepared to work only in areas where Wi-Fi connectivity is available, which is usually the case in residential and commercial areas. Additionally, as discussed in the previous section, the device can occasionally reboot, leading to data losses. Including external storage could solve the latter problem. However, the ESP32 would require an external oscillator crystal to keep the system time up to date without an NTP server since the internal oscillator caused delays up to 20 seconds per hour.

Inconsistencies in this work are present in the selection criteria of the electronic components. For some components, the availability in the Energy Technology Laboratory or the practicality was prioritized over the price, even though a low overall cost was a specification of the desired device. Also, the software code can be slightly inconsistent in style because of the author’s initial inexperience in C programming.

As for the consistencies, the device was designed strongly considering all the requirements. Also, the hardware design follows a common logic and the PCB layout style is the same for both PCBs.

9 Conclusion

Installing residential and commercial photovoltaic systems is a growing tendency (IRENA, 2021) but usually requires a feasibility study and scenario evaluation to guarantee cost-effectiveness and optimal solar energy utilisation.

In this thesis, a low-cost solar data logger has been developed to provide empirical data on available solar power to evaluate potential areas for solar energy harvesting. The device is based on an ESP32 SoC and uses a 5 W PV panel to obtain statistics on generated PV power. The manufacturing cost of a prototype is estimated to be about 75 €. This price compares favourably to near commercial devices such as the model presented by Rocha et al. (2021) for non-meteorological purposes.

The partial I-V characteristics of the PV panel are the primary data used as an indicator of the ideality of the irradiance and temperature conditions for solar power generations. The characterisation process is done by using a MOSFET as a variable electronic load and an INA219 as a current and voltage sensor. A characterisation speed under five seconds with a resolution of 64 I-V points is achieved.

The logger device is battery powered, and the software is optimised for battery saving, reaching an autonomy of about 40 days with a measurement period of 5 minutes or 70 days with 10 minutes. The device also uses the PV panel as a sensor and an energy source to recharge the battery when needed. Solar energy harvesting is common in wireless sensor nodes but not for data loggers, often powered externally.

The proposed device does not use an external storage unit. Instead, it periodically logs the data to an MQTT broker. For this reason, the device can only be used in areas with Wi-Fi connectivity. Wi-Fi connectivity is also used to update the system time and reliably obtain daylight hours.

This thesis enables further study and development possibilities. Firstly, after obtaining measurement data for all irradiances and different temperature conditions (a data pool of several months), processing the information and analysing whether the measured magnitudes can provide enough information to reliably determine the ideality of an area for a PV installation would validate the concept of this work. Secondly, if the concept is validated, the device can be further developed by further reducing the cost, increasing the integration, improving the velocity and reliability of the measurements, and enabling long-term offline functioning.

In conclusion, the aim and objectives of this thesis were almost entirely fulfilled. A data logger that copes with the initially set requirements has been designed and partially manufactured. Only the final 3D printing of the case and assembly of the device is missing, having all the CAD designs for printed parts ready.

10 References

Apogee Instruments (n.d.). *Silicon-cell Pyranometers and Meters*. [online] www.apogeeinstruments.com. Available at: https://www.apogeeinstruments.com/silicon-cell-pyranometers/ [Accessed 16 Jul. 2022].

Atonometrics (2013). *PV Reference Cell*. [online] www.atonometrics.com. Available at: https://www.atonometrics.com/pv-reference-cell/ [Accessed 10 Aug. 2022].

Battery University (2021). *BU-808: How to Prolong Lithium-based Batteries*. [online] Battery University. Available at: https://batteryuniversity.com/article/bu-808-how-to-prolong-lithium-based-batteries [Accessed 1 Aug. 2022].

Chang, C., Schultz, A. and Surtihadi, H. (2018). *Precise Photovoltaic I-V Characterization*. [online] Analog Devices. Available at: https://www.analog.com/en/technical-articles/precise-photovoltaic-i-v-characterization.html.

Chen, Y.J., Hu, C., Sun, Y.Z. and Meng, Z. (2012). Development of a Low Cost Device for Measuring Solar Irradiance. *Advanced Materials Research*, [online] 457-458, pp.1377–1382. doi:10.4028/www.scientific.net/AMR.457-458.1377.

Choudhary, A., Pandey, D. and Bhardwaj, S. (2020). Overview of Solar Radiation Estimation Techniques with Development of Solar Radiation Model Using Artificial Neural Network. Advances in Science, Technology and Engineering Systems Journal, 5(4), pp.589–593. doi:10.25046/aj050469.

Cruz-Colon, J., Martinez-Mitjans, L. and Ortiz-Rivera, E.I. (2012). *Design of a low cost irradiance meter using a photovoltaic panel*. [online] IEEE Xplore. doi:10.1109/PVSC.2012.6318195.

Crystal, G. (2022). *What is Data Logging?* [online] EasyTechJunkie. Available at: https://www.easytechjunkie.com/what-is-data-logging.htm [Accessed 15 Jul. 2022].

DanKoloff and TsvetanUsunov (2020). *ESP32-DevKit-LiPo*. [online] Github. Available at: https://github.com/OLIMEX/ESP32-DevKit-LiPo.git [Accessed 31 Jul. 2022].

de Barros, R.C., Callegari, J.M.S., Mendonca, D. do C., Amorim, W.C.S., Silva, M.P. and Pereira, H.A. (2018). *Low-Cost Solar Irradiance Meter using LDR Sensors*. [online] IEEE Xplore. doi:10.1109/INDUSCON.2018.8627176.

de Sousa, I.R., de Oliveira Segundo, R.V., de Sá Medeiros, C.M. and Silva, E.T. (2018). *Estimation of global solar irradiance with LDR sensor and artificial neural network embedded in an 8-bit microcontroller*. [online] IEEE Xplore. doi:10.1109/IJCNN.2018.8489206.

Dokter, P. (2013). *SparkFun According to Pete #34: PCB Layout*. [online] YouTube. Available at: https://www.youtube.com/watch?v=NJKZZArjdg8 [Accessed 31 Jul. 2022].

DroneBot Workshop (2021). *Getting Started with PlatformIO*. *YouTube*. Available at: https://www.youtube.com/watch?v=JmvMvIphMnY&t=1400s [Accessed 1 Aug. 2022].

Duran, E., Piliougine, M., Sidrach-de-Cardona, M., Galan, J.A. and Marquez, A. (2008). Different methods to obtain the I–V curve of PV modules: A review. In: *Conference Record of the IEEE Photovoltaic Specialists Conference*. pp.1–6. doi:10.1109/PVSC.2008.4922578.

Effendi, A., Dewi, A.Y. and Ismail, F. (2018). Data Logger Development to Evaluate Potential Area of Solar Energy. *MATEC Web of Conferences*, [online] 215, p.01014. doi:10.1051/matecconf/201821501014.

Espressif Systems (2022). *ESP32 Series Datasheet*. [online] Available at: https://www.espressif.com/sites/default/files/documentation/esp32_datasheet_en.pdf [Accessed 17 Jul. 2022].

Forero, N., Hernández, J. and Gordillo, G. (2006). Development of a monitoring system for a PV solar plant. *Energy Conversion and Management*, [online] 47(15), pp.2329–2336. doi:10.1016/j.enconman.2005.11.012.

GlobalSpec (2020). *Measuring the differences: Shunt-based sensing technology vs. magnetic solutions*. [online] electronics360.globalspec.com. Available at: https://electronics360.globalspec.com/article/15270/measuring-the-differences-shunt-based-sensing-technology-vs-magnetic-solutions [Accessed 30 Jul. 2022].

He, Y., Li, Y., Liu, L. and Wang, L. (2009). Solar micro-power system for self-powered wireless sensor nodes. In: J. Tan and X. Wen, eds., *International Society for Optics and Photonics*. [online] SPIE, p.71333Z. doi:10.1117/12.810134.

Hlapisi, N. (2021). *Understanding the Difference Between BJT and MOSFET and How to Select the Right One for Your Designs*. [online] circuitdigest.com. Available at: https://circuitdigest.com/article/understanding-the-difference-between-bjt-and-mosfet-and-how-to-select-the-right-one-for-your-designs [Accessed 30 Jul. 2022].

Honsberg, C. and Bowden, S. (2019a). *Electronics*. [online] Photovoltaics Education Website. Available at: https://www.pveducation.org [Accessed 29 Jul. 2022].

Honsberg, C. and Bowden, S. (2019b). *Module Circuit Design*. [online] Photovoltaics Education Website. Available at: https://www.pveducation.org [Accessed 28 Jul. 2022].

Honsberg, C. and Bowden, S. (2019c). *Module Measurement with Load*. [online] Photovoltaics Education Website. Available at: https://www.pveducation.org [Accessed 28 Jul. 2022].

Honsberg, C. and Bowden, S. (2019d). *Nominal Operating Cell Temperature*. [online] Photovoltaics Education Website. Available at: https://www.pveducation.org [Accessed 29 Jul. 2022].

Hukseflux Thermal Sensors (2017). *Pyranometers versus PV reference cells in outdoor PV system performance monitoring*. [online] *www.hukseflux.com*. Available at: https://www.hukseflux.com/uploads/inline/white_paper_pyranometers_versus_pv_reference_cells_v1717.pdf [Accessed 16 Jul. 2022].

Hukseflux Thermal Sensors (2018a). *Hukseflux pyranometer selection guide*. [online] *www.hukseflux.com*. Available at: https://www.hukseflux.com/uploads/inline/selection_guide_hukseflux_pyranometers_v1833_0.pdf [Accessed 30 Jul. 2022].

Hukseflux Thermal Sensors (2018b). *PV monitoring and meteorological industries prepare for revised pyranometer standard ISO 9060:2018*. [online] Available at: https://www.hukseflux.com/uploads/inline/how_to_prepare_for_the_revised_pyranometer_standard_iso_9060-2018_v1812.pdf [Accessed 30 Jul. 2022].

Hukseflux Thermal Sensors (2020). *What is a pyranometer?* [online] *www.hukseflux.com*. Available at: https://www.hukseflux.com/uploads/inline/note-what_is_a_pyranometer_v2006.pdf [Accessed 16 Jul. 2022].

Hukseflux Thermal Sensors (2021). *USER MANUAL SR05-D1A3 & SR05-D2A2*. [online] *www.hukseflux.com*. Available at: https://www.hukseflux.com/uploads/product-documents/SR05-D1A3_%26_SR05-D2A2_manual_v2120.pdf [Accessed 16 Jul. 2022].

Infineon Technologies (n.d.). *IRLZ34NPbF*. [online] Available at: https://www.infineon.com/dgdl/irlz34npbf.pdf?fileId=5546d462533600a4015356720689 2720 [Accessed 30 Jul. 2022].

IRENA (2021), Renewable Power Generation Costs in 2020, International Renewable Energy Agency, Abu Dhabi

Jones, D. (2004). *PCB Design Tutorial*. [online] Available at: http://alternatezone.com/electronics/files/PCBDesignTutorialRevA.pdf [Accessed 13 May 2022].

Keim, R. (2015). *Beyond the DMM: Components and Circuits for Measuring Current and Voltage*. [online] www.allaboutcircuits.com. Available at: https://www.allaboutcircuits.com/technical-articles/beyond-the-dmm-components-and-circuits-for-measuring-current-and-voltage/ [Accessed 30 Jul. 2022].

Kim, D.-R., Kang, J.-W., Eom, T.-H., Kim, J.-M., Lee, J. and Won, C.-Y. (2018). Rapid-charging solution for 18650 cylindrical lithium-ion battery packs for forklifts. *Journal of Electrochemical Science and Technology*, 9, pp.184–194. doi:10.33961/JECST.2018.9.3.184.

Kuai, Y. and Yuvarajan, S. (2006). An electronic load for testing photovoltaic panels. *Journal of Power Sources*, 154(1), pp.308–313. doi:10.1016/j.jpowsour.2005.04.016.

Leibson, S. (2018). *Fundamentals of Current Measurement: Part 1 – Current Sense Resistors*. [online] Digi-Key Electronics. Available at: https://www.digikey.de/en/articles/fundamentals-of-current-measurement-part-1-current-sense-resistors [Accessed 31 Jul. 2022].

Liang, S., Li, X. and Wang, J. (2012). *Advanced remote sensing*. Amsterdam; Boston: Academic Press.

Martínez, M., Andújar, J. and Enrique, J. (2009). A New and Inexpensive Pyranometer for the Visible Spectral Range. *Sensors*, [online] 9(6), pp.4615–4634. doi:10.3390/s90604615.

Maxim Integrated (2019). *DS18B20*. [online] Available at: https://datasheets.maximintegrated.com/en/ds/DS18B20.pdf [Accessed 31 Jul. 2022].

Meydbray, J., Emery, K. and Kurtz, S. (2012a). *Pyranometers and Reference Cells, What's the Difference?* [online] www.osti.gov. Available at: https://www.osti.gov/biblio/1038336-pyranometers-reference-cells-what-difference-preprint [Accessed 16 Jul. 2022].

Meydbray, J., Riley, E., Dunn, L., Emery, K. and Kurtz, S. (2012b). *Pyranometers and Reference Cells: Part 2: What Makes the Most Sense for PV Power Plants?; Preprint*. [online] *www.osti.gov*. Available at: https://doi.org/10.2172/1059158 [Accessed 16 Jul. 2022].

NOVUS Automation (n.d.). *NOVUS Automation Inc.* [online] www.novusautomation.com. Available at: https://www.novusautomation.com/site/ [Accessed 15 Jul. 2022].

Oliveira, A., Jerome, B., Vermeulen, L. and Borek, N. (n.d.). *User Manual of a Low-Cost Pyranometer*. [online] Available at: http://images.shoutwiki.com/mindworks/e/e6/The_Solar_Sailors_User_Manual.pdf [Accessed 16 Jul. 2022].

OMEGA Engineering (2018). *Data Loggers*. [online] https://www.omega.com/en-us/resources/data-loggers. Available at: https://www.omega.com/en-us/resources/data-loggers [Accessed 15 Jul. 2022].

OptoSupply Limited (n.d.). *OSTA5131A-C*. [online] Available at: https://www.tme.eu/Document/b520efa483e2260c9cb894ee426ff830/osta5131a-c.pdf [Accessed 31 Jul. 2022].

Pace Scientific (n.d.). *Data Loggers and Sensors - Pace Scientific*. [online] www.pace-sci.com. Available at: https://www.pace-sci.com/ [Accessed 15 Jul. 2022].

Palo-Tejada, E., Campos-Falcon, V., Merma, M. and Huanca, E. (2020). Low-cost data logging device to measure irradiance based on a Peltier cell and artificial neural networks. *Journal of Physics: Conference Series*, 1433(1), p.012008. doi:10.1088/1742-6596/1433/1/012008.

Pérez GarcíaM.A. (2014). *Instrumentación electrónica*. Madrid: Paraninfo, Cop.

Rao, R.J.M. (2021). *What are Analog and Digital Signals? Differences, Examples*. [online] Inst Tools. Available at: https://instrumentationtools.com/what-are-analog-and-digital-signals-differences-examples/ [Accessed 30 Jul. 2022].

Rocha, Á.B. da, Fernandes, E. de M., Santos, C.A.C. dos, Diniz, J.M.T. and Junior, W.F.A. (2021). Development of a Real-Time Surface Solar Radiation Measurement System Based on the Internet of Things (IoT). *Sensors*, [online] 21(11), p.3836. doi:10.3390/s21113836.

RS Components (1997). *Light dependent resistors*. [online] Available at: https://components101.com/sites/default/files/component_datasheet/LDR%20Datasheet.pdf [Accessed 16 Jul. 2022].

Sahbel, A., Hassan, N., Abdelhameed, M.M. and Zekry, A. (2013). Experimental Performance Characterization of Photovoltaic Modules Using DAQ. *Energy Procedia*, [online] 36, pp.323–332. doi:10.1016/j.egypro.2013.07.037.

Shanghai Belling (2009). *BL4054/BL4054B*. [online] Available at: https://datasheet.lcsc.com/lcsc/1810010135_BL-Shanghai-Belling-BL4054B-42TPTRN_C194062.pdf [Accessed 28 Jul. 2022].

Sharko, G., Hobdari, N., Shanku, N., Ekmekciu, M. and Dasho, E. (2011). Photovoltaic module V-I and P-V characterization through instrumentation control toolkit of MATLAB. *Perspectives of Innovations, Economics and Business*, 9(3), pp.72–77. doi:10.15208/pieb.2011.44.

Silergy Corp (n.d.). *Application Note: AN_SY8089/SY8089A*. [online] Available at: https://datasheet.lcsc.com/szlcsc/Silergy-Corp-SY8089AAAC_C78988.pdf [Accessed 28 Jul. 2022].

smartswitchsio (2018). *Programming Languages for ESP32 & ESP8266*. [online] ElectronicDIYs. Available at: https://www.electronicdiys.com/2018/11/programming-languages-for-esp32-esp8266.html [Accessed 1 Aug. 2022].

SolarEdge (n.d.). *Designer | Gratis SolarEdge solar design software tool*. [online] www.solaredge.com. Available at: https://www.solaredge.com/nl/products/installer-tools/designer#/ [Accessed 11 Apr. 2022].

Spiess, A. (2020). *#340 How good are the ADCs inside Arduinos, ESP8266, and ESP32? And external ADCs (ADS1115)*. *YouTube*. Available at: https://www.youtube.com/watch?v=UAJMLTzrM9Q [Accessed 28 Jul. 2022].

Spiess, A. (2021). *#387 Test of Battery operated ESP32 Boards (Olimex, TinyPICO, EzSBC, TTGO)*. *YouTube*. Available at: https://www.youtube.com/watch?v=ajt7vtgKNNM&t=280s [Accessed 28 Jul. 2022].

Tassell, C. and Maule, D.J. (2002). Photodiode arrays — Characteristics and applications. *Microelectronics Journal*, [online] 10(1), pp.35–44. doi:10.1016/s0026-2692(79)80096-8.

Texas Instruments Incorporated (2015). *INA219 Zerø-Drift, Bidirectional Current/Power Monitor With I 2C Interface*. [online] Available at: https://www.ti.com/lit/ds/symlink/ina219.pdf?ts=1659162655734&ref [Accessed 30 Jul. 2022].

Tohsing, K., Phaisathit, D., Pattarapanitchai, S., Masiri, I., Buntoung, S., Aumporn, O. and Wattan, R. (2019). A development of a low-cost pyranometer for measuring broadband solar radiation. *Journal of Physics: Conference Series*, [online] 1380(1), p.012045. doi:10.1088/1742-6596/1380/1/012045.

Trace Software International (n.d.). *Solar PV Design Software*. [online] Trace Software. Available at: https://www.trace-software.com/archelios-pro/solar-pv-design-software/ [Accessed 11 Apr. 2022].

University of Illinois at Urbana-Champaign (n.d.). *Solar Cells and Photodiodes*. [online] courses.engr.illinois.edu. Available at: https://courses.engr.illinois.edu/ece110/fa2020/content/courseNotes/files/?photodiodes [Accessed 16 Jul. 2022].

Vera, L.H., Busso, A.J. and Benítez, F. (2005). Piranómetro fotovoltaico con sistema autónomo de adquisición de datos. *Avances en Energías Renovables y Medio Ambiente*, [online] vol. 9, pp.7–12. Available at: http://sedici.unlp.edu.ar/handle/10915/82861 [Accessed 10 Aug. 2022].

Villalva, M., Gazoli, J. and Filho, E. (2009). Comprehensive approach to modeling and simulation of photovoltaic arrays. *Power Electronics, IEEE Transactions on*, 24, pp.1198–1208. doi:10.1109/TPEL.2009.2013862.

Will Semiconductor Ltd. (2018). *WPM2015*. [online] Available at: https://datasheet.lcsc.com/lcsc/1808311550_WILLSEMI-Will-Semicon-WPM2015-3-TR_C213159.pdf [Accessed 28 Jul. 2022].

Zhang, D., Liu, Y., Li, J., Xue, C.J., Li, X., Wang, Y. and Yang, H. (2016). Solar Power Prediction Assisted Intra-task Scheduling for Nonvolatile Sensor Nodes. *IEEE Transactions on Computer-Aided Design of Integrated Circuits and Systems*, [online] 35(5), pp.724–737. doi:10.1109/TCAD.2016.2527710.

Appendix 1

Calculations of a resistor-based signal amplifier (by a factor lower than the unity) and offset circuit for high input impedance purposes.

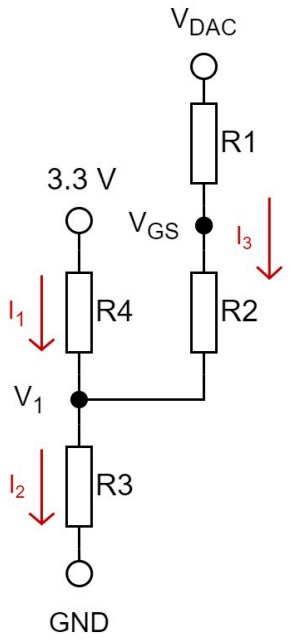

Applying Kirchhoff's current law on the V_1 node and then applying Ohm's law to each current, [1] can be obtained.

$$I_1 + I_3 = I_2 \rightarrow \frac{3.3 - V_1}{R_4} + \frac{V_{DAC} - V_1}{R_1 + R_2} = \frac{V_1}{R_3} \quad [1]$$

By unifying the denominator on the left side of [1], [2] is obtained:

$$\frac{(3.3 - V_1)(R_1 + R_2) + (V_{DAC} - V_1)R_4}{R_4(R_1 + R_2)} = \frac{V_1}{R_3} \quad [2]$$

If [2] is modified to an expression of voltages with coefficients based on resistances, [4] is obtained through [3]:

$$3.3R_1 + 3.3R_2 - V_1R_1 - V_1R_2 + V_{DAC}R_4 - V_1R_4 = \frac{R_4}{R_3}(R_1 + R_2)V_1 \quad [3]$$

$$3.3(R_1 + R_2) + V_{DAC}R_4 = V_1\left(\frac{R_4}{R_3}(R_1 + R_2) + R_1 + R_2 + R_4\right) \quad [4]$$

If V_1 is isolated from [4], [5] is obtained:

$$V_1 = \frac{3.3(R_1 + R_2) + V_{DAC}R_4}{\left(\frac{R_4}{R_3}(R_1 + R_2) + R_1 + R_2 + R_4\right)} \quad [5]$$

Expressing V_{GS} ad a function of V_1, [6] is obtained:

$$V_{GS} = V_{DAC} - I_3 R_1 = V_{DAC} - R_1 \frac{V_{DAC} - V_1}{R_1 + R_2} = V_{DAC}\left(1 - \frac{R_1}{R_1 + R_2}\right) + V_1 \frac{R_1}{R_1 + R_2} \quad [6]$$

Substituting [5] in [6], [7] is obtained:

$$V_{GS} = V_{DAC}\left(1 - \frac{R_1}{R_1 + R_2}\right) + \frac{R_1}{R_1 + R_2} \frac{3.3(R_1 + R_2) + V_{DAC} R_4}{\left(\frac{R_4}{R_3}(R_1 + R_2) + R_1 + R_2 + R_4\right)} \quad [7]$$

Imposing correlative conditions to V_{DAC} and V_{GS} in [7], a two-equation system with two degrees of liberty can be obtained. The system must be solved for R1, R2, R3, and R4, assuming the value of two of the four resistances. The necessary conditions for this work are:

$$\begin{cases} V_{DAC} = 0.07\ V \rightarrow V_{GS} = 1.6\ V \\ V_{DAC} = 3.2\ V \rightarrow V_{GS} = 2.4\ V \end{cases}$$

The equation system has been solved in MATLAB with the following script:

```
%% Assume R1 and R3 and calculate R2 and R4.
R1 = 560000;
R3 = 68000;
Vdac_min = 0.07; % DAC output for the value 0x00
Vdac_max = 3.2; % DAC output for the value 0xFF
Vgs_min = 1.6;
Vgs_max = 2.4;
Vcc = 3.3;
syms R2 R4 real positive
eq1 = Vgs_min == Vdac_min + R1/(R1+R2)*((Vcc*(R1+R2) +
Vdac_min*R4)/(R4/R3*(R1+R2)+R1+R2+R4) - Vdac_min);
eq2 = Vgs_max == Vdac_max + R1/(R1+R2)*((Vcc*(R1+R2) +
Vdac_max*R4)/(R4/R3*(R1+R2)+R1+R2+R4) - Vdac_max);

R = solve([eq1,eq2],"Real",true);
fprintf("R2: %.0f\n",eval(R.R2));
fprintf("R4: %.0f\n",eval(R.R4));

%% Assign R2 and R4 and recalculate V_GS range.
R2 = 180000;
R4 = 39000;
Vg = @(Vdac) Vdac + R1/(R1+R2)*((Vcc*(R1+R2) +
Vdac*R4)/(R4/R3*(R1+R2)+R1+R2+R4) - Vdac);
Vgs_min = Vg(Vdac_min);
Vgs_max = Vg(Vdac_max);
fprintf("Vg_min: %.2f\n",Vgs_min);
fprintf("Vg_max: %.2f\n",Vgs_max);
```

Values for R1 and R3 are assumed and the ideal values for R2 and R4 are calculated in the first part of the script. Then R2 and R4 are manually assumed close to the calculated values and the range of V_{GS} is recalculated and must be checked I it is close enough to the initially desired value.

Appendix 2

Schematic of the main circuit of the data logger.

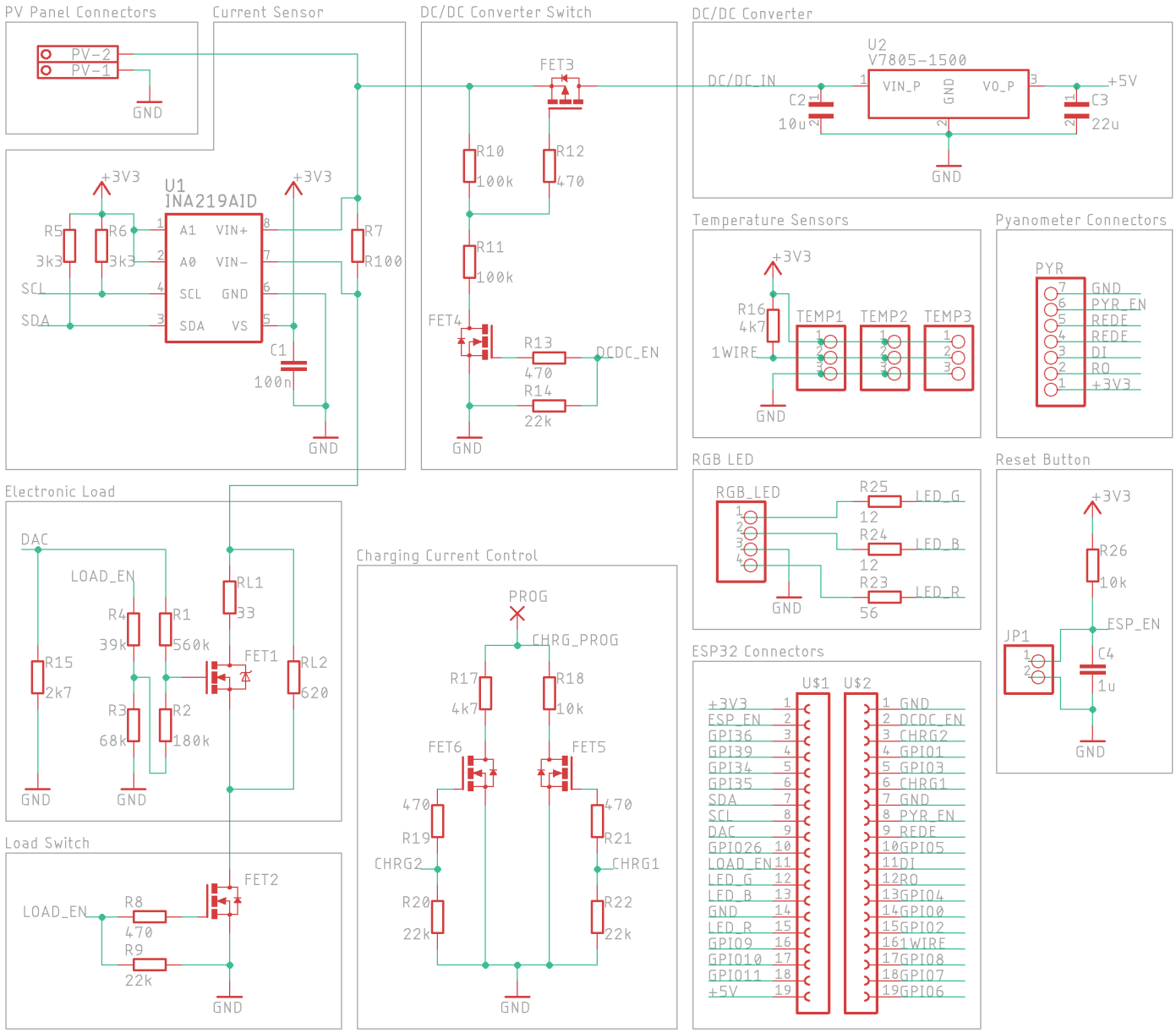

Appendix 3

List of components for the main circuit of the solar logger.

Part	Device	Value	Package	Description
C1	C1206C104K5RACTU	100n	1206	Ceramic capacitor
C2	TMK316AB7106KL-T	10u	1206	Ceramic capacitor
C3	EMK316BJ226KL-T	22u	1206	Ceramic capacitor
C4	C1206C105K3RACTU	1u	1206	Caramic capacitor
R1	RTT065603F	560k	1206	Thick film resistor
R2	RTT061803F	180k	1206	Thick film resistor
R3	RTT066802F	68k	1206	Thick film resistor
R4	RTT063902F	39k	1206	Thick film resistor
R5	RTT063301F	3k3	1206	Thick film resistor
R6	RTT063301F	3k3	1206	Thick film resistor
R7	CRA2512-FZ-R100ELF	R100	2512	Current sense resistor
R8	RTT064700F	470	1206	Thick film resistor
R9	RTT062202F	22k	1206	Thick film resistor
R10	RTT061003F	100k	1206	Thick film resistor
R11	RTT061003F	100k	1206	Thick film resistor
R12	RTT064700F	470	1206	Thick film resistor
R13	RTT064700F	470	1206	Thick film resistor
R14	RTT062202F	22k	1206	Thick film resistor
R15	RTT062701F	2k7	1206	Thick film resistor
R16	RTT064701F	4k7	1206	Thick film resistor
R17	RTT064701F	4k7	1206	Thick film resistor
R18	RTT061002F	10k	1206	Thick film resistor
R19	RTT064700F	470	1206	Thick film resistor
R20	RTT062202F	22k	1206	Thick film resistor
R21	RTT064700F	470	1206	Thick film resistor
R22	RTT062202F	22k	1206	Thick film resistor
R23	RTT0656R0F	56	1206	Thick film resistor
R24	RTT0612R0F	12	1206	Thick film resistor
R25	RTT0612R0F	12	1206	Thick film resistor
R26	RTT061002F	10k	1206	Thick film resistor
RL1	ROX5SSJ33R	33	N/A	Power resistor
RL2	ROX5SSJ620R	620	N/A	Power resistor
FET1	IRLZ34NPBF	N/A	TO-220AB	N-channel enhancement MOSFET
FET2	DMN3150L-7	N/A	SOT-23-3	N-channel enhancement MOSFET
FET3	DMP3130LQ-7	N/A	SOT-23-3	P-channel enhancement MOSFET
FET4	DMN3150L-7	N/A	SOT-23-3	N-channel enhancement MOSFET
FET5	DMN3150L-7	N/A	SOT-23-3	N-channel enhancement MOSFET
FET6	DMN3150L-7	N/A	SOT-23-3	N-channel enhancement MOSFET
U1	INA219AIDR	N/A	SOIC-8	Current/power monitor
U2	V7805-1500	N/A	TO-220-3	Buck converter
JP1	PR2.54-40S	N/A	N/A	1x19 pin socket, 2.54mm pitch
JP2	PR2.54-40S	N/A	N/A	1x19 pin socket, 2.54mm pitch
PV	19963	N/A	N/A	1x2 screw terminal, 3.5mm pitch
JP1	PR-40PK (partial)	N/A	N/A	1x2 pin header, 2.54mm pitch
PYR	PR-40PK (partial)	N/A	N/A	1x7 pin header, 2.54mm pitch
RGB_LED	PR-40PK (partial)	N/A	N/A	1x4 pin header, 2.54mm pitch

Appendix 4

Schematic of the pyranometer module for the solar logger.

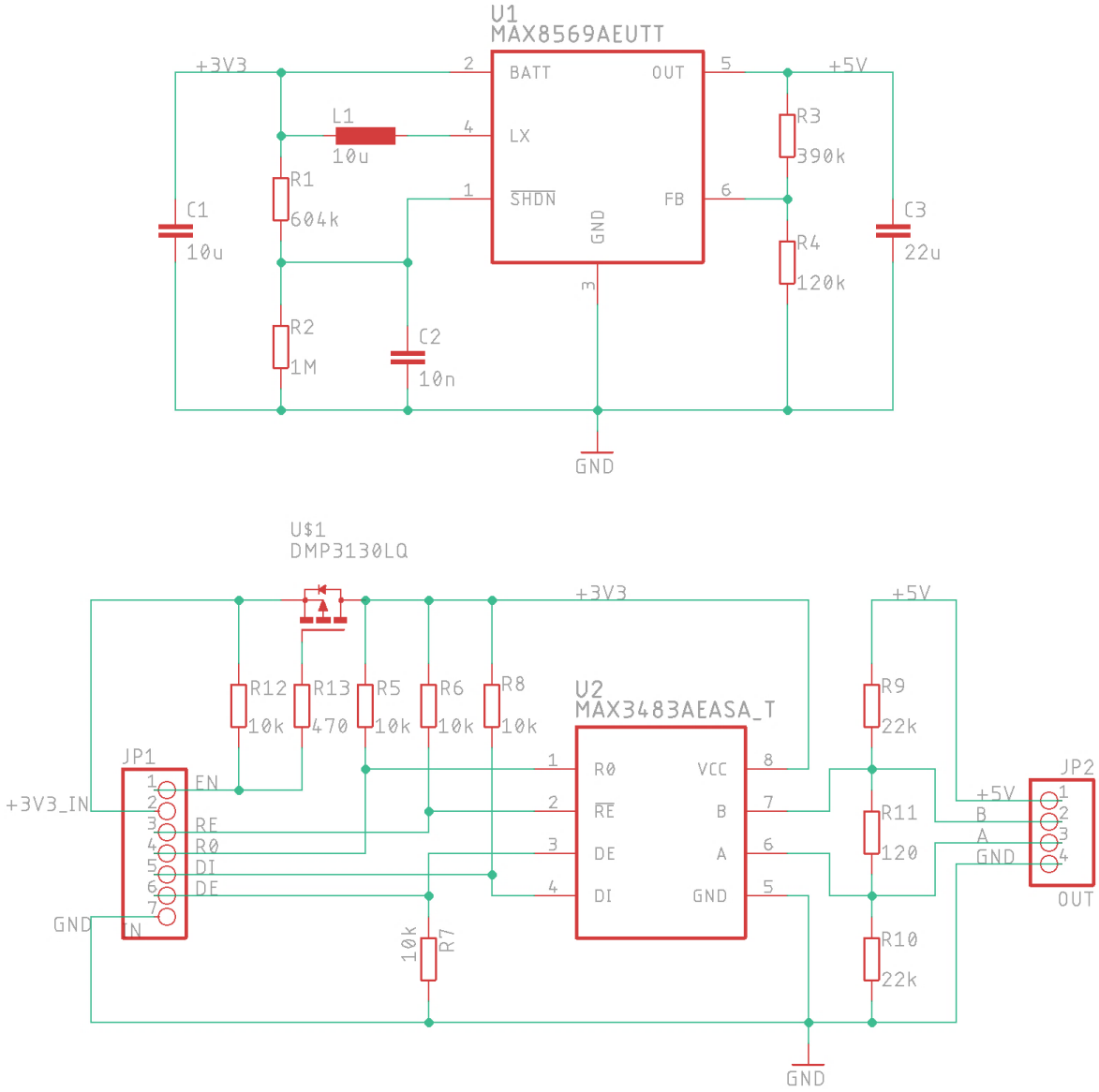

Appendix 5

List of components for the pyranometer module for the solar logger.

Part	Device	Value	Package	Description
C1	C1206C106K4PACTU	10u	1206	Ceramic capacitor
C3	C1206C226M8PACTU	22u	1206	Ceramic capacitor
L1	744042100	10u	Custom	Inductor
R1	RTT063903F	390k	1206	Thick film resistor
R2	RTT061203F	120k	1206	Thick film resistor
R3	RTT061002F	10k	1206	Thick film resistor
R4	RTT061002F	10k	1206	Thick film resistor
R5	RTT061002F	10k	1206	Thick film resistor
R6	RTT061002F	10k	1206	Thick film resistor
R7	RTT062202F	22k	1206	Thick film resistor
R8	RTT061004F	1M	1206	Thick film resistor
R9	RTT062202F	22k	1206	Thick film resistor
R10	RTT062202F	22k	1206	Thick film resistor
R11	RTT061200F	120	1206	Thick film resistor
FET1	DMP3130LQ-7	N/A	SOT-23-3	P-channel enhancement MOSFET
U1	MAX8569AEUT+T	N/A	SOT-23-6	Step-up converter
U2	MAX3483AEASA+T	N/A	SOIC-8	RS-485 transceiver
JP1	PR-40PK (partial)	N/A	N/A	1x7 pin header, 2.54mm pitch
JP2	PR-40PK (partial)	N/A	N/A	1x4 pin header, 2.54mm pitch

Appendix 6

Cost of the electronic components for the main circuit

Device	Description	Qty.	PPU	Min. Qty.	Distributor	Price
ESP32-Devkit-Lipo	ESP32 development board	1	9.95 €	1	Olimex	9.95 €
JA-803450P	1400 mAh LiPo battery	1	5.95 €	1	Olimex	5.95 €
Eco Line ES5P36	Polycrystalline 5W PV panel	1	13.95 €	1	Amazon	13.95 €
DS18B20	Temp. sensor	3	1.2657 €	1	LCSC	3.7971 €
OSTA5131A-C	RGB LED	1	0.83 €	1	Starelec Oy	0.83 €
PTS645SM43SMTR92LFS	Tactile switch	1	0.1075 €	5	LCSC	0.1075 €
PR-40PK	1x40 pin header, 2.54mm pitch	1	0.4100 €	1	Starelec Oy	0.4100 €
PR2.54-40S	1x40 pin socket, 2.54mm pitch	1	0.31 €	1	Starelec Oy	0.31 €
19963	1x2 screw terminal, 3.5mm pitch	1	0.59 €	5	Adafruit	0.59 €
V7805-1500	Buck converter	1	9.13 €	1	Mouser	9.13 €
INA219AIDR	Current/power monitor	1	2.68 €	1	Farnell	2.68 €
DMN3150L-7	N-channel enhancement MOSFET	4	0.593 €	5	Farnell	2.372 €
DMP3130LQ-7	P-channel enhancement MOSFET	1	0.50 €	1	Mouser	0.50 €
IRLZ34NPBF	N-channel enhancement MOSFET	1	1.62 €	1	Mouser	1.62 €
ROX5SSJ33R	33Ω power resistor	1	0.616 €	1	Farnell	0.616 €
ROX5SSJ620R	620Ω power resistor	1	0.616 €	1	Farnell	0.616 €
CRA2512-FZ-R100ELF	0.1Ω shunt resistor	1	0.61 €	1	Mouser	0.61 €
RTT0612R0F	12Ω SMR	2	0.0041 €	100	LCSC	0.0082 €
RTT0656R0F	56Ω SMR	1	0.0041 €	100	LCSC	0.0041 €
RTT064700F	470Ω SMR	5	0.0041 €	50	LCSC	0.0205 €
RTT062701F	2.7kΩ SMR	1	0.0051 €	50	LCSC	0.0051 €
RTT063301F	3.3kΩ SMR	2	0.0062 €	50	LCSC	0.0124 €
RTT064701F	4.7kΩ SMR	2	0.0041 €	100	LCSC	0.0082 €
RTT061002F	10kΩ SMR	2	0.0045 €	50	LCSC	0.0090 €
RTT062202F	22kΩ SMR	4	0.0059 €	50	LCSC	0.0236 €
RTT063902F	39kΩ SMR	1	0.0048 €	50	LCSC	0.0048 €
RTT066802F	68kΩ SMR	1	0.0054 €	50	LCSC	0.0054 €
RTT061003F	100kΩ SMR	2	0.0052 €	50	LCSC	0.0104 €
RTT061803F	180kΩ SMR	1	0.0065 €	50	LCSC	0.0065 €
RTT065603F	560kΩ SMR	1	0.0065 €	50	LCSC	0.0065 €
C1206C104K5RACTU	100nF ceramic cap.	1	0.16 €	1	Mouser	0.16 €
C1206C105K3RACTU	1uF ceramic cap.	1	0.28 €	1	Mouser	0.28 €
TMK316AB7106KL-T	10uF ceramic cap.	1	0.33 €	1	Mouser	0.33 €
EMK316BJ226KL-T	22uF ceramic cap.	1	0.59 €	1	Mouser	0.59 €
					TOTAL	**55.52 €**

Cost of the optional pyranometer module (excluding the pyranometer)

Device	Description	Qty.	PPU	Min. Qty.	Distributor	Price
MAX8569AEUT+T	Step-up converter	1	2.79 €	1	Farnell	2.79 €
MAX3483AEASA+T	RS-485 transceiver	1	5.46 €	1	Mouser	5.46 €
DMP3130LQ-7	P-channel enhancement MOSFET	1	0.50 €	1	Mouser	0.50 €
744042100	10uH inductor	1	1.53 €	1	Mouser	1.53 €
C1206C106K4PACTU	10uF ceramic cap.	1	0.38 €	1	Mouser	0.38 €
C1206C226M8PACTU	22uF ceramic cap.	1	0.51 €	1	Mouser	0.51 €
RTT061200F	120Ω SMR	1	0.0076 €	50	LCSC	0.0076 €
RTT061002F	10kΩ SMR	4	0.0045 €	50	LCSC	0.0180 €
RTT062202F	22kΩ SMR	3	0.0059 €	50	LCSC	0.0177 €
RTT061203F	120kΩ SMR	1	0.0037 €	100	LCSC	0.0037 €
RTT063903F	390kΩ SMR	1	0.0066 €	50	LCSC	0.0066 €
RTT061004F	1MΩ SMR	1	0.0049 €	50	LCSC	0.0049 €
					TOTAL	**11.23 €**